The Meteoritical Society

Meteoritics & Planetary Science 59, Nr 12, 3282–3304 (2024)
doi: 10.1111/maps.14276

Radial transport and nebular thermal processing of millimeter-sized solids in the Solar protoplanetary disk inferred from Cr-Ti-O isotope systematics of chondrules

Kohei FUKUDA[1,2]*, Yuki HIBIYA[3,4], Craig R. KASTELLE[5], Katsuhiko SUZUKI[4], Tsuyoshi IIZUKA[6], Katsuyuki YAMASHITA[7], Thomas E. HELSER[5], and Noriko T. KITA[1]

[1]WiscSIMS, Department of Geoscience, University of Wisconsin-Madison, Madison, Wisconsin, USA
[2]Forefront Research Center, Graduate School of Science, Osaka University, Toyonaka, Osaka, Japan
[3]Research Center for Advanced Science and Technology, Graduate School of Science, The University of Tokyo, Meguro, Tokyo, Japan
[4]Submarine Resources Research Center, Japan Agency for Marine-Earth Science Technology, Yokosuka, Kanagawa, Japan
[5]National Oceanic and Atmospheric Administration, Seattle, Washington, USA
[6]Department of Earth and Planetary Science, Graduate School of Science, The University of Tokyo, Bunkyo, Tokyo, Japan
[7]Graduate School of Environmental, Life, Natural Science and Technology, Okayama University, Okayama, Okayama, Japan

***Correspondence**
Kohei Fukuda, Forefront Research Center, Graduate School of Science, Osaka University, 1-1 Machikaneyama-cho, Toyonaka-shi, Osaka 560-0043, Japan.
Email: kfukuda@ess.sci.osaka-u.ac.jp

(Received 29 March 2024; revision accepted 09 October 2024)

Abstract–Understanding the material transport and mixing processes in the Solar protoplanetary disk provides important constraints on the origin of chemical and isotopic diversities of our planets. The limited extent of radial transport and mixing between the inner and outer Solar System has been suggested based on a fundamental isotopic dichotomy between non-carbonaceous (NC) and carbonaceous (CC) meteorite groups. The limited transport and mixing could be further tested by tracing the formation regions of individual meteoritic components, such as Ca-Al-rich inclusions (CAIs) and chondrules. Here, we show further evidence for the outward transport of CAIs and chondrules from the inner and subsequent thermal processing in the outer region of the protoplanetary disk based on the petrography and combined Cr-Ti-O isotope systematics of chondrules from the Vigarano-like (CV) carbonaceous chondrite Allende. One chondrule studied consists of an olivine core that exhibits NC-like Ti and O, but CC-like Cr isotopic signatures, which is enclosed by a pyroxene igneous rim with CC-like O isotope ratios. These observations indicate that the olivine core formed in the inner Solar System. The olivine core then migrated into the outer Solar System and experienced nebular thermal processing that generated the pyroxene igneous rim. The nebular thermal processing would result in Cr isotope exchange between the olivine core and CC-like materials, but secondary alteration effects on the parent body are also responsible for the CC-like Cr isotope signature. By combining previously reported Cr-Ti-O isotope systematics of CV chondrules, we show that some CV chondrules larger than ~1 mm would have formed in the inner Solar System. The accretion of the millimeter-sized, inner Solar System solids onto the CV carbonaceous chondrite parent body would require their very early migration into the outer Solar System within the first 1 million years after the Solar System formation.

INTRODUCTION

Astronomical observations and dynamical modeling reveal that radial transport and mixing of materials within a given protoplanetary disk could occur during the earliest epoch of the disk evolution (e.g., Cuzzi et al., 2010; Watson et al., 2009). In our Solar System, it is known that comets contain gas–solid condensates that formed at high temperatures in the early Solar System (e.g., Defouilloy et al., 2017; Fukuda et al., 2021; Joswiak et al., 2017; Nakashima et al., 2012). Since comets are thought to have formed in cold, outer disk regions, the presence of gas–solid condensates thus required large-scale outward transport of the inner Solar System materials (Bockelée-Morvan et al., 2002; Ciesla, 2007). It is also well established that primitive, undifferentiated meteorites, namely, chondrites, contain Ca-Al-rich inclusions (CAIs) that are the oldest solids in our Solar System (Amelin et al., 2010; Bouvier & Wadhwa, 2010; Connelly et al., 2012), which are believed to have formed in hot, innermost regions in the Solar protoplanetary disk, likely within ~1 astronomical unit (AU) from the Sun (Krot, 2019; MacPherson, 2014; Shu et al., 1996; Wood, 2004). CAIs are often observed in carbonaceous chondrites, for which parent asteroids have accreted in the outer Solar System (>3 astronomical units; AU; Desch et al., 2018), suggesting outward transport of CAIs from the innermost part after their formation (Wood, 2004). Such radial transport may play pivotal roles in originating chemical and isotopic diversities among Solar System objects. For instance, nucleosynthetic Ca and Fe isotope anomalies among inner Solar System bodies, including Earth, suggest that inward migration of outer Solar System materials would have occurred throughout ~5 million years (Ma) after CAIs, which could induce temporal changes of chemical and isotopic compositions of the inner Solar System bodies that likely formed within <3 AU (Desch et al., 2018; Schiller et al., 2018, 2020). Thus, deciphering the nature of radial transport processes sheds light on the origin and evolution of our Solar System objects.

Nucleosynthetic isotope variability among meteorites and their components, which reflects the heterogeneous distribution of the distinct products from various nucleosynthetic sources, can be used to track their formation locations and subsequent migration in the Solar protoplanetary disk. High-precision isotope analyses of bulk meteorites reveal a fundamental isotopic dichotomy between non-carbonaceous (NC) and carbonaceous (CC) meteorite groups, which is often considered to reflect distinct formation regions of each meteorite group, that is, inner and outer Solar System, respectively (e.g., Bermingham et al., 2020; Budde et al., 2016; Kleine et al., 2020; Trinquier et al., 2009; Warren, 2011; hereafter the inner and outer Solar System correspond the disk regions inside and outside 3 AU, respectively; Desch et al., 2018). Radiometric dating and thermal modeling suggest that the two distinct isotope reservoirs have coexisted during a period of ~2 Ma after CAIs (Kleine et al., 2020; Kruijer et al., 2020 and references therein). The coexistence of the two isotope reservoirs implies that they were separated by a physical barrier caused either by the presence of proto-Jupiter (Kruijer et al., 2017) or H_2O snow line (Lichtenberg et al., 2021), although the origin of the physical barrier is actively debated (e.g., Brasser & Mojzsis, 2020; Lichtenberg et al., 2021). The presence of the physical barrier would have inhibited significant mixing of materials between the inner and outer Solar System (Spitzer et al., 2020).

Recent isotope studies of mm-sized solids, namely, chondrules, which are the major components of chondrites, give rise to a question regarding the limited mixing between these two reservoirs. Oxygen isotope analyses of chondrules from carbonaceous chondrites reveal the presence of rare chondrules/fragments with NC-like O isotope signatures (e.g., Schrader et al., 2020; Tenner et al., 2017; Zhang et al., 2022). In addition to oxygen isotopes, the similarity in mineral chemistry of chondrules/fragments in ordinary chondrites and interplanetary dust particles, as well as those in comet 81P/Wild 2, also supports the outward migration of high-temperature components from the inner to the outer Solar System (Brownlee & Joswiak, 2017; Frank et al., 2014; Schrader & Davidson, 2022; Zhang et al., 2021, 2024). Further, chondrules from Vigarano-like (CV) carbonaceous chondrites exhibit large isotope variabilities in Cr, Ti, and O isotopes, some of which have NC-like isotope signatures (Connelly et al., 2012; Gerber et al., 2017; Hertwig et al., 2018; Hertwig, Kimura, Defouilloy, et al., 2019; Olsen et al., 2016; Schneider et al., 2020; Trinquier et al., 2007, 2009; van Kooten et al., 2021; Williams et al., 2020). The presence of NC-like materials in the carbonaceous chondrites indicates that large-scale outward transport occurred before the accretion of the carbonaceous chondrite parent asteroids. However, the timing and efficiency of outward transport remain to be better defined. Knowledge of the timing and efficiency of outward transport is central to elucidating the origin of the chemical and isotopic diversities among the Solar System bodies. In this study, we conducted detailed petrographic and in situ O isotope investigations as well as combined Cr and Ti isotope analyses of chondrules from the Allende meteorite (CV3.6; Bonal et al., 2006). By combining the results with previously reported Cr-Ti-O isotope data, we discuss the timing of outward transport of millimeter-sized objects from the inner Solar System.

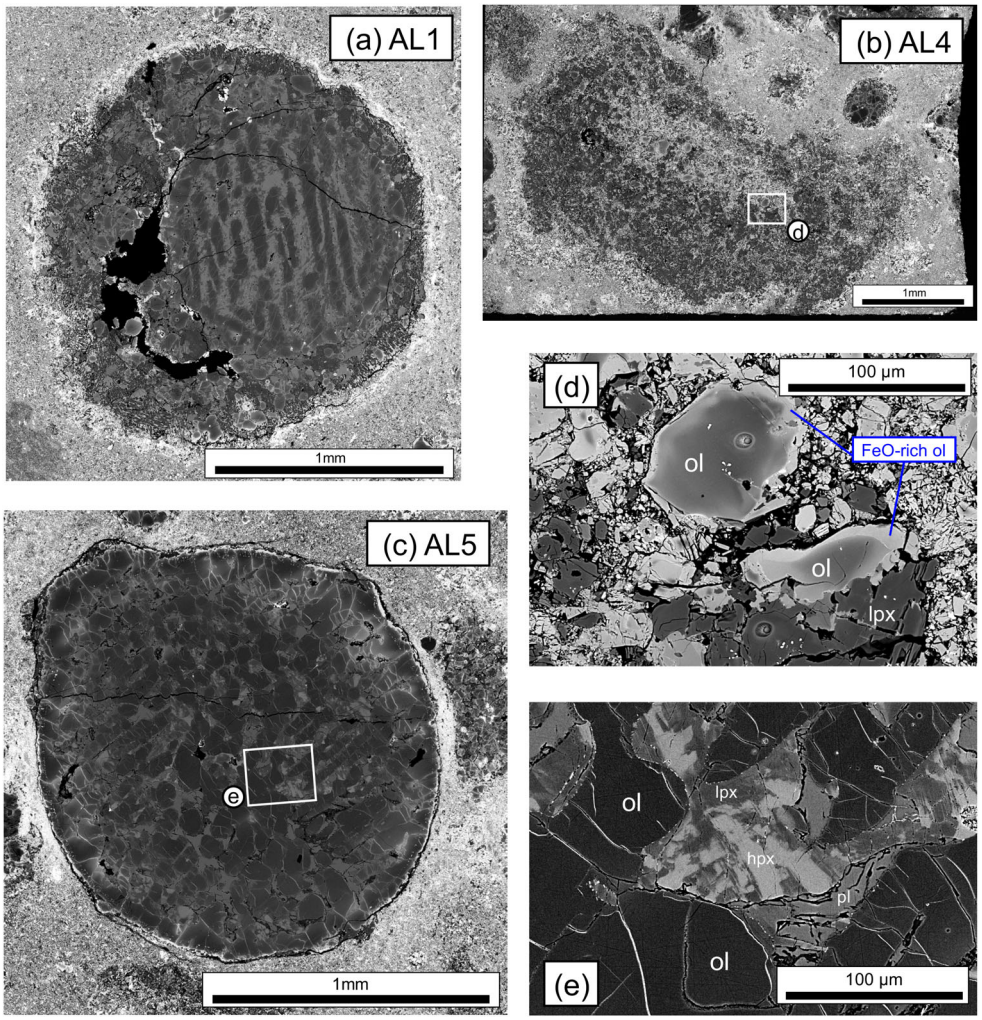

FIGURE 1. Backscattered electron images of chondrules from the Allende (CV3.6) carbonaceous chondrite. White rectangles in (b) and (c) indicate areas shown as expanded views in (d) and (e), respectively. (a) Enveloping compound chondrule AL1 (BO + POP, Mg# = 98). (b) Chondrule AL4 (POP, Mg# = 98). (c) Chondrule AL5 (PO, Mg# = 92). Mineral phases shown are olivine (ol), low-Ca pyroxene (lpx), high-Ca pyroxene (hpx), and plagioclase (pl). (Color figure can be viewed at wileyonlinelibrary.com)

MATERIALS AND METHODS

We prepared 20 thick sections (~100 mm^2, ~0.5 mm thickness each) of the carbonaceous chondrite Allende (CV3.6; Bonal et al., 2006) and selected 5 chondrules (Figures 1–3) for isotope analyses. During the preparation of thick sections, we observed the front and back sides of 20 slices of the Allende slab (USNM 3509-10) with a Hitachi S-3400 scanning electron microscope (SEM) at the University of Wisconsin-Madison, to confirm that a given chondrule is visible at both front and back sides of a given slice (Figure S1). These 20 slices were then embedded in epoxy and polished. The five chondrules were selected that are larger than 1.5 mm in diameter (Table 1), which potentially allows precise Cr and Ti isotope analyses of individual chondrules. All five chondrules were investigated for their oxygen isotope ratios, and three of them (AL1, AL2, AL3) were further investigated for their Cr and Ti isotope ratios. The Mg#, where Mg# = [MgO]/[MgO + FeO] mole%, of the five chondrules was determined using the Hitachi S-3400 SEM with an energy dispersive spectrometer (EDS). The EDS analyses were the standardless measurements, and thus the reported Mg#s are semiquantitative. The uncertainties on Mg#s reported here are better than 1 based on the comparison between EDS and EPMA results (Material S1 and Tenner et al., 2017).

Oxygen three-isotope analyses of individual minerals (olivine, pyroxene, plagioclase, spinel) in the five chondrules were performed with a Cameca IMS 1280 secondary ion mass spectrometer (SIMS) at the University of Wisconsin, Madison. The analytical

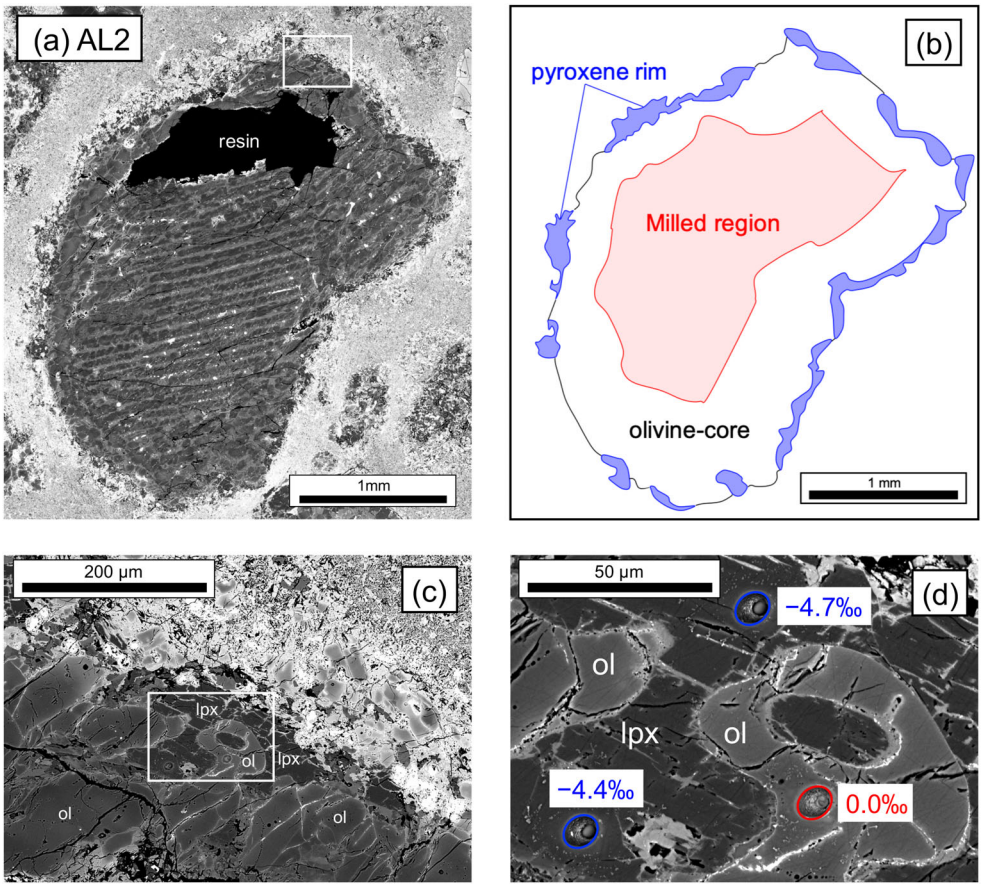

FIGURE 2. (a) Backscattered electron image of chondrule AL2 (BO, Mg# = 98). This chondrule consists of the olivine-rich core that is enclosed by the pyroxene igneous rim (b). White rectangles in (a) and (c) indicate areas shown as expanded views in (c) and (d), respectively. $\Delta^{17}O$ values of individual SIMS spot analyses are also shown in (d). A milled region for Cr and Ti isotope analyses is indicated as red filed in (b). Scales for (a) and (b) are the same. Mineral phases shown are olivine (ol) and low-Ca pyroxene (lpx). (Color figure can be viewed at wileyonlinelibrary.com)

conditions are similar to those described in Siron et al. (2021). A $^{133}Cs^+$ primary ion beam was focused to 12 × 10 μm in diameter at 2 nA, resulting in secondary ion intensities of ~2.3 × 10^9 cps (counts per second) for $^{16}O^-$ on San Carlos olivine (SC-Ol) measurements. Secondary ions ($^{16}O^-$, $^{17}O^-$, $^{18}O^-$) were detected simultaneously using multi-collector Faraday cups (FC) (Kita et al., 2010). Additionally, $^{16}O^1H^-$ was detected at the end of each measurement in order to estimate the potential tailing effect on the $^{17}O^-$ signal (Heck et al., 2010), which was found to be insignificant (<0.02‰ on $\delta^{17}O$; Table S2). The mass resolving power was set to ~2200 for $^{16}O^-$ and $^{18}O^-$, and ~5000 for $^{17}O^-$. To improve the precision of ^{17}O measurements, the FC for $^{17}O^-$ employed a high-gain feedback resistor (10^{12} ohm) that can reduce thermal noise (Fukuda et al., 2021). The other FCs for $^{16}O^-$ and $^{18}O^-$ employed 10^{10} and 10^{11} ohm resistors, respectively. The SC-Ol reference material ($\delta^{18}O$ = 5.32‰; Kita et al., 2010) was used as the bracketing standard. The external reproducibility of the bracketing standard was typically 0.2‰ for $\delta^{18}O$ and 0.3‰ for $\delta^{17}O$ and $\Delta^{17}O$ (2 standard deviations; 2SD). Three additional olivine, as well as five pyroxene, one plagioclase, and one spinel reference materials, were analyzed to correct instrumental mass fractionation, of which $\delta^{18}O$ values have been determined by laser fluorination analyses (Fukuda et al., 2020; Kita et al., 2010; Zhang et al., 2022). Data for standard analyses, instrumental biases, and calibration curves for each mineral are presented in Tables S1–S4.

After the SIMS O isotope analyses, three chondrules, AL1, AL2, and AL3, were extracted from the thick sections using a diamond drill bit equipped with a micro-milling system (*Carpenter Systems CM-2*; Kastelle et al., 2017) at the Alaska Fishery Science Center, National Oceanic and Atmospheric Administration (NOAA). The other two chondrules (AL4 and AL5) were not extracted because AL4 exhibits evidence of extensive thermal metamorphism (see the Results section). Further, AL5 is the smallest one among the chondrules we studied

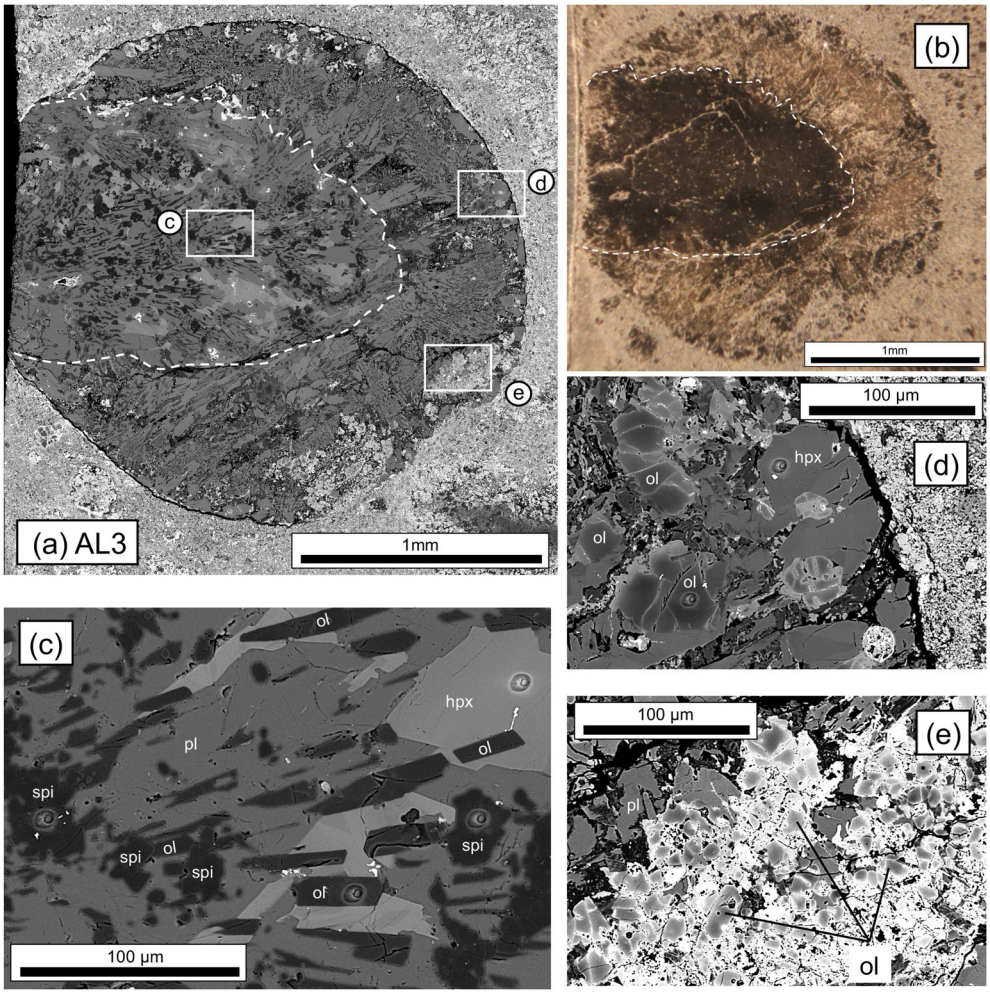

FIGURE 3. (a) Backscattered electron image of chondrule AL3 (Al-rich, Mg# = 99). This chondrule exhibits a core–mantle structure, which is clearly seen in an optical microscopic image (b). White rectangles in (a) indicate areas shown as expanded views in (c), (d), and (e), respectively. Mineral phases shown are spinel (spi), olivine (ol), high-Ca pyroxene (hpx), and plagioclase (pl). (Color figure can be viewed at wileyonlinelibrary.com)

here, for which mass may not be enough for sufficient high-precision (0.1ε) ^{54}Cr and ^{50}Ti isotope analyses (minimum masses required are 12 μg Cr and 4 μg Ti; Hibiya et al., 2019), so we kept it for future higher precision Cr and Ti isotope analyses. Before the milling of individual chondrules, we first removed surrounding matrix materials with chondrule periphery in order to avoid any contamination from the matrix ("matrix removal"). After the matrix removal, the thick section and diamond drill bit were cleaned in a sonic cleaner with Milli-Q water. For the milling of a chondrule itself, a droplet of Milli-Q water was placed on the given chondrule to avoid scattering of the sample powder during the milling (Charlier et al., 2006). The chondrule milling was conducted under the water droplet, which was then collected with a pipette and placed in 3 mL Savillex® PFA vial. Optical microscopic images of the milled areas were taken before and after matrix removal, and after chondrule milling, to verify any contamination from the surrounding matrix (Figures S2–S4).

The milled chondrules (AL1, AL2, and AL3) in vials were then heated on a hotplate and evaporated to dryness. Subsequently, the samples were digested with 1.2 mL of concentrated HF and 0.9 mL of concentrated HNO_3 in a Parr bomb at 200°C for >65 h. The digested samples were converted to soluble compounds by repeated evaporation with concentrated HNO_3 and finally re-dissolved in 1 mL of 6 mol L^{-1} HCl on a 140°C hotplate. Both Cr and Ti were separated from the digested sample following the procedure described in Hibiya et al. (2019), using AG1-X8 anion exchange resin (200–400 mesh), TODGA resin (200–400 mesh), and AG50W-X8 cation exchange resin (100–200 mesh). All Cr isotopic compositions of the separated samples were obtained by a TIMS (Thermo Fisher Scientific, TRITON Plus) at the Japan Agency for Marine-Earth Science Technology, Japan, following the

TABLE 1. Size, Mg#s, and oxygen isotope ratios of five chondrules from Allende (CV3.6) carbonaceous chondrite.

Chondrule	Type	Diameter (mm)	Pyroxene Mg#[a]				Olivine Mg#				Mean oxygen isotope ratios					
			Mean	+	−	N	Mean	+	−	N	$\delta^{18}O$	Unc.[b]	$\delta^{17}O$	Unc.[b]	$\Delta^{17}O$	Unc.[b]
AL1	Type I, BO + POP	1.7	98.4	0.4	0.7	7	94.8	0.3	2.7	24	−1.91	0.44	−5.10	0.35	−4.10	0.20
AL2[c]	Type I, BO	2.5	98.4	0.6	0.8	9	94.9	2.8	5.5	23	3.44	0.36	1.70	0.24	−0.09	0.16
AL3	Al-rich	2.2	98.5	1.4	2.1	36	94.7	4.6	23	34	−13.09	3.27	−16.24	3.37	−9.43	1.72
AL4	Type I, POP	2.8	97.6	0.8	0.8	21	84.0	9.7	22.8	18	−1.20	0.34	−4.31	0.25	−3.68	0.15
AL5	Type I, PO	1.5	92.4	0.9	0.7	8	91.0	2.7	11.5	37	3.54	0.32	1.83	0.24	−0.01	0.19

[a]Mean Mg# of each chondrule is taken as the average of low-Ca pyroxene, except for chondrule AL3. For chondrule AL3, the average is calculated from high-Ca-pyroxene since it contains no low-Ca pyroxene. Uncertainties represent the range in measured Mg#s.
[b]Quoted uncertainties are at 2σ level for AL1, AL2, AL4, and AL5, while those for AL3 are 2SD. See Text and Supplementary materials S1 for more details.
[c]Mean oxygen isotope ratios are calculated from olivine analyses.

method described in Yamakawa et al. (2009). All Cr isotopic ratios are presented as relative deviation from the NIST-979 Cr standard in standard epsilon notation: $\varepsilon^{n}Cr = [(^{n}Cr/^{52}Cr)_{sample}/(^{n}Cr/^{52}Cr)_{ref} - 1] \times 10^{4}$. The Ti isotopic compositions were obtained using an MC-ICP-MS (Thermo Fisher Scientific, Neptune Plus) at the Japan Agency for Marine-Earth Science Technology. The sample solutions with concentrations of about 500 ppb were introduced via a CETAC Aridus-II desolvating nebulizer. Individual sample measurements were bracketed by analyses of a NIST SRM 3162a standard solution. The instrumental mass bias was corrected by using an exponential law relative to $^{49}Ti/^{47}Ti = 0.749766$ (Leya et al., 2007). It has been shown that NIST SRM 3162a has excesses of 0.04 ± 0.21, −0.10 ± 0.21, 0.28 ± 0.17 of ^{46}Ti, ^{48}Ti, and ^{50}Ti relative to Alfa Aesar Ti standard solution that is widely used in meteorite Ti isotope studies (Zhang et al., 2011). For comparison with literature values, all Ti isotopic ratios of samples are presented in the ε unit as relative deviations from the Alfa Aesar standard solution, as follows: $\varepsilon^{n}Ti = [(^{n}Ti/^{47}Ti)_{sample}/(^{n}Ti/^{47}Ti)_{NIST3162a} - 1] \times 10^{4}$ + (0.04 for $\varepsilon^{46}Ti$, −0.10 for $\varepsilon^{48}Ti$, 0.28 for $\varepsilon^{50}Ti$) (n = 46, 48, 50). Errors of both Cr and Ti isotope ratios were propagated to include the "internal errors" and the uncertainty in the isotope normalization to the reference materials.

RESULTS

Research data of this study [SIMS O isotope data (Tables S1–S4) and mineral chemistry obtained with SEM-EDS (Table S5)] are summarized in Material S2. Positions of SIMS O isotope analyses are shown in Material S3.

Petrography and Mineral Chemistry

The five chondrules studied here include a compound chondrule that consists of barred olivine (BO) + porphyritic olivine pyroxene (POP) (BO + POP; AL1, Figure 1a), a POP (AL4, Figure 1b), a porphyritic olivine (PO; AL5, Figure 1c), a BO (AL2, Figure 2), and an Al-rich (AL3, Figure 3). All chondrules but AL3 are classified as type I ferromagnesian chondrules (Mg# > 90) that are mainly composed of olivine and low-Ca pyroxene. The Mg# of low-Ca pyroxene grains in the 4 type I chondrules spans from 92 to 99 and exhibits a narrow range within each chondrule (±1 units; Table 1). In contrast, their olivine grains tend to show lower and more variable Mg#s within each chondrule (Table 1), suggesting that olivine Mg#s were modified by Fe-Mg diffusion during thermal metamorphism on the parent body (e.g., Hertwig, Kimura, Defouilloy, et al., 2019). Thus, we refer to pyroxene Mg#s as a representative Mg# for the chondrules we studied. Petrographic information for each chondrule is summarized below.

The BO + POP chondrule AL1 (Mg# = 98) appears to be an enveloping compound chondrule consisting of a primary BO chondrule surrounded by a secondary POP shell (Figure 1a). Both BO and POP portions consist of olivine, pyroxene, and plagioclase. The enveloping compound petrography indicates that this chondrule experienced at least two melting episodes (e.g., Rubin, 1984, 2010; Wasson et al., 1995).

The POP chondrule AL4 (Mg# = 98) consists of an olivine-rich core that is enclosed by a pyroxene-rich mantle (Figure 1b). This chondrule appears to have experienced extensive metasomatic alteration. Olivine grains exhibit the lowest mean Mg# = 84 and the largest variation in Mg#s ranging from 61 to 94 among the chondrules studied, which are substantially lower than those of coexisting pyroxene grains (Mg# = 98). FeO-rich olivine forms rim on relatively FeO-poor olivine phenocrysts (Figure 1d). These observations suggest that chondrule AL4 has suffered thermal metamorphism on the parent body, which induced Mg-Fe diffusion in olivine phenocrysts and the formation of FeO-rich olivine rims (Krot et al., 1995, 1998).

The PO chondrule AL5 (Mg# = 92) is composed mostly of olivine and minor amounts of low-Ca and high-Ca pyroxenes and plagioclase (Figure 1c,e). Some olivine grains appear to have a skeletal texture (Figure 1c). The observed mineralogical occurrence is very similar to that of large (>4 mm) Allende chondrules studied by Connelly et al. (2012) (see their supplementary materials), in which ε^{54}Cr values are negative.

The BO chondrule AL2 (Mg# = 98) consists of an olivine-rich core with minor amounts of pyroxene and plagioclase, which is enclosed by a low-Ca pyroxene igneous rim (Figure 2a,b). The observed minerals of the olivine-rich core and their textural occurrence are similar to those of the primary BO chondrule in AL1.

The Al-rich chondrule AL3 (Mg# = 99) is composed of calcic plagioclase, Al-Ti-rich pyroxene (hpx in Figure 3), spinel, olivine, and nepheline (Figure 3a). This chondrule appears to have a core–mantle structure according to an optical microscopic image (Figure 3b). Plagioclase and Al-Ti-rich pyroxene grains are distributed throughout the chondrule. Spinel grains are only observed in the core. Two texturally different generations of olivine are observed: locally oriented lath-shaped olivine in the core (Figure 3c) and PO assemblages in the mantle (Figure 3d,e). As for the other 4 chondrules we studied, Mg#s of pyroxene grains are fairly homogeneous (Mg# = 99 ± 2) over the chondrule but those of olivine grains are more heterogeneous (72 < Mg# < 99; mean Mg# = 95). Of the core, corroded spinel grains are enclosed by other minerals such as plagioclase, olivine, and Al-Ti-rich pyroxene (Figure 3c). Lath-shaped olivine grains are enclosed by plagioclase and Al-Ti-rich pyroxene (Figure 3c). The observed textural relationships indicate that a crystallization sequence of the core minerals is spinel → olivine → Al-Ti-rich pyroxene → plagioclase. The mantle portion is mainly composed of Al-Ti-rich pyroxene and plagioclase with small amounts of PO grains (Figure 3d). Nepheline and sodalite are also present throughout the mantle and could be secondary alteration products.

Oxygen Isotope Ratios

Individual O isotope analyses of chondrule minerals are reported in Table S4 and are plotted in Figure 4. Three out of the five chondrules (AL1, AL4, AL5) are internally homogeneous with O isotope ratios, except for two analyses of chondrule AL4 (Figure 4a–c). Thus, we calculate the mean O isotope ratios of the three chondrules by averaging multiple olivine and pyroxene analyses. The calculation procedure can be found in Material S1. In an oxygen three-isotope diagram, two olivine analyses of chondrule AL4 deviate from the rest of the analyses (Figure 4b and Table S4), which could be O isotopic relict grains. Another possibility is O isotope exchange with relatively ^{16}O-depleted fluid during metasomatic alteration on the parent body, which is more likely because of its extensive altered features, as described above. In fact, Δ^{17}O values and Mg#s of the two olivine grains are ^{16}O-depleted and lower than relative to the others, respectively, supporting this possibility (Material S2). In either case (relict or metamorphism), the two olivine grains may not record original O isotope ratios when they crystallized, so these data were not included for calculating mean O isotope ratios of chondrule AL4.

The other two chondrules (AL2, AL3) show O isotope heterogeneity among coexisting minerals (Figure 4d,e). In chondrule AL2, O isotope ratios of olivine are homogeneous (Δ^{17}O = −0.1 ± 0.2; 2SD), but are systematically ^{16}O-depleted compared with those of pyroxene igneous rim (Δ^{17}O = −4.6 ± 0.3; 2SD). It is noteworthy that O isotope ratios of olivine grains are homogeneous throughout chondrule AL2, including some rounded olivine grains that seem to be residues of partial melting to form the igneous pyroxene rim (Figure 2c,d). We refer to O isotope ratios of olivine as mean O isotope ratios of chondrule AL2 since olivine is the major constituent mineral of this chondrule, and pyroxene grains that are relatively ^{16}O-rich compared with olivine grains are found only at chondrule periphery as the igneous rim (Figure 2b). The Al-rich chondrule AL3 shows a large heterogeneity in O isotope ratios (Figure 4e). Spinel and plagioclase are the most ^{16}O-rich ($-23.9 \leq \Delta^{17}O \leq -20.9$; Figure 4f) and ^{16}O-depleted ($-2.6 \leq \Delta^{17}O \leq -2.2$; Figure 4e) among coexisting minerals, respectively. Δ^{17}O values of olivine and Al-Ti-rich pyroxene are intermediate ($-10.8 \leq \Delta^{17}O \leq -8.2$; Figure 4g). The average Δ^{17}O values (± 2SD) of spinel, olivine, Al-Ti-rich pyroxene, and plagioclase are −22.7 ± 3.11 (N = 3), −9.53 ± 2.10 (N = 4), −9.37 ± 1.63 (N = 7), and − 2.37 ± 0.45 (N = 3), respectively. A systematic O isotope difference in the core and mantle is found, that is, olivine and Al-Ti-rich pyroxene in the core are enriched in ^{16}O compared with those in the mantle (Figure 4h). We consider that spinel grains are relict, and plagioclase grains experienced O isotope exchange with ^{16}O-depleted metasomatic fluid on the CV parent body (e.g., Hertwig, Kimura, Defouilloy, et al., 2019; Krot et al., 2019). In this case, spinel and plagioclase do not record O isotope ratios of host chondrule melt. Therefore, we refer to average O isotope ratios of all olivine and pyroxene analyses as mean O isotope ratios of chondrule AL3. Since olivine and pyroxene exhibit a resolvable variation in Δ^{17}O beyond the 3SD external reproducibility, we assign 2SD of all

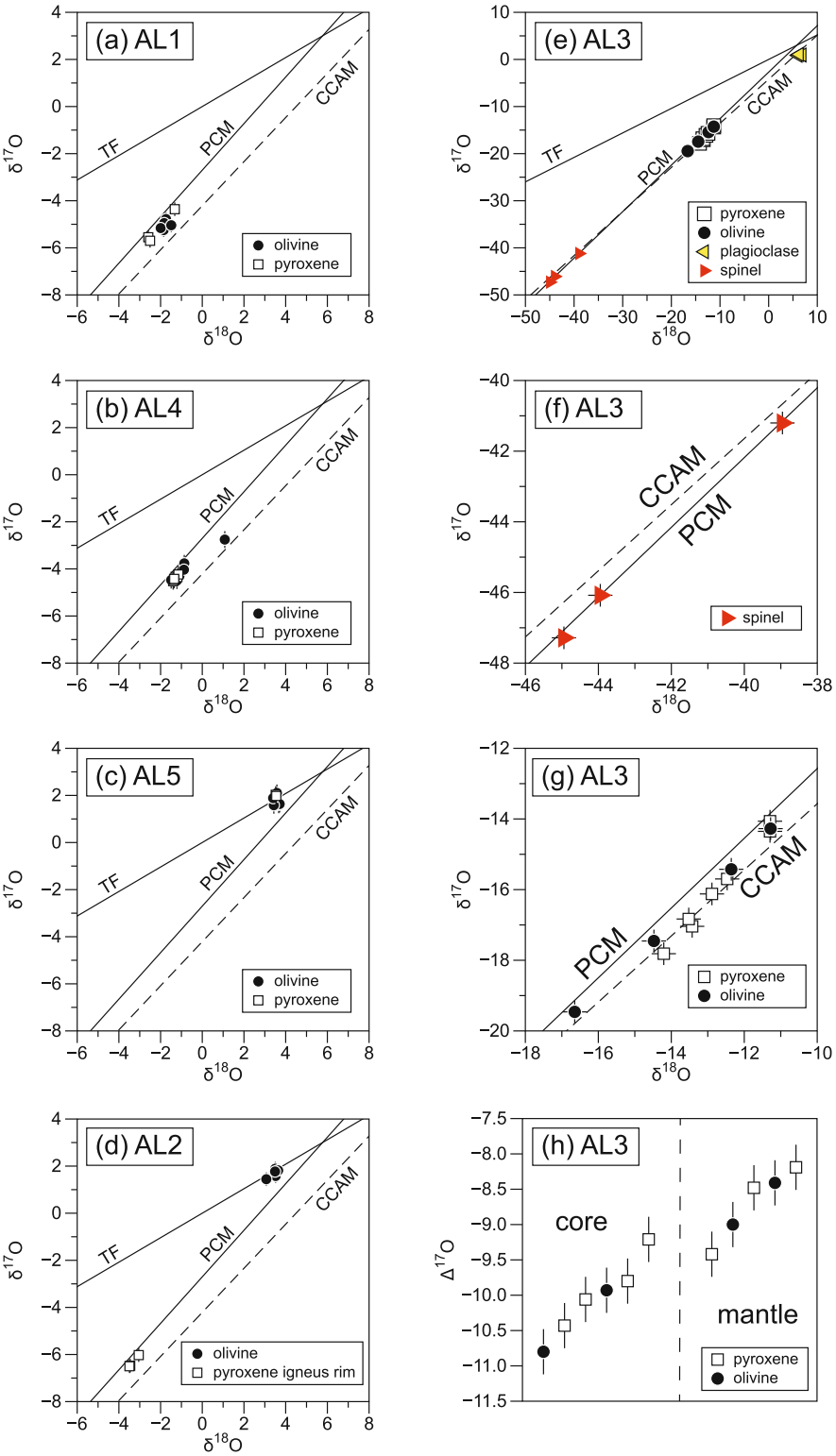

FIGURE 4. Oxygen three-isotope diagrams for (a) enveloping compound chondrule AL1 (BO + POP), (b) chondrule AL4 (POP), (c) chondrule AL5 (PO), (d) chondrule AL2 (BO), (e) Al-rich chondrule AL3. (f) The enlarged view for spinel analyses in (e). (g) The enlarged view for olivine and pyroxene analyses in (e). (h) $\Delta^{17}O$ values of olivine and pyroxene analyses in (g). Olivine and pyroxene grains in the core are systematically enriched in ^{16}O compared with those in the mantle. Reference lines are terrestrial fractionation (TF; Clayton et al., 1991), Primitive Chondrule Minerals (PCM; Ushikubo et al., 2012), and Carbonaceous Chondrite Anhydrous Mineral (CCAM; Clayton et al., 1977) lines. (Color figure can be viewed at wileyonlinelibrary.com)

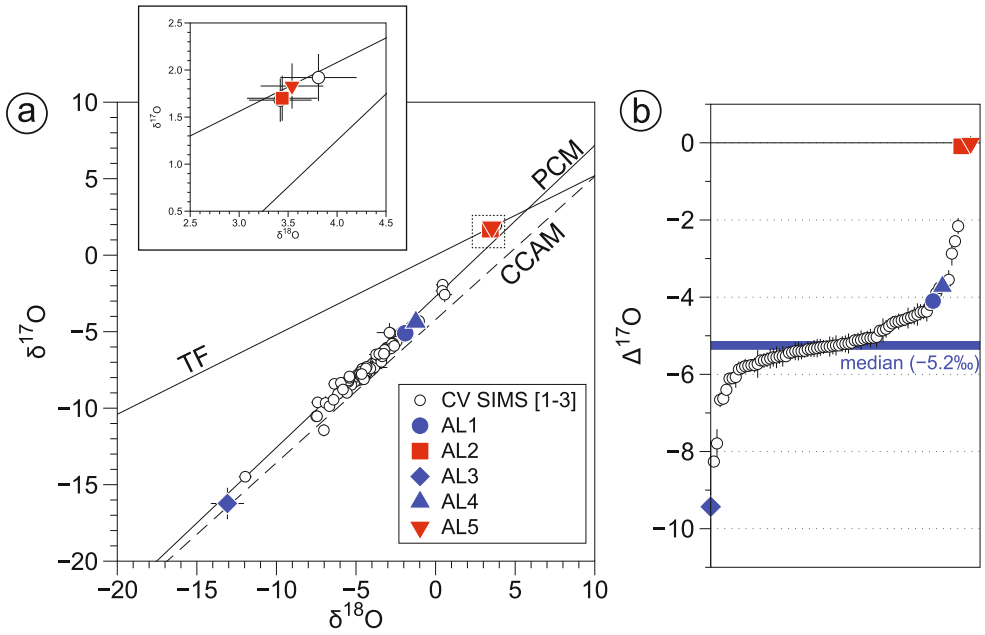

FIGURE 5. Mean oxygen isotope ratios of individual type I chondrules from CV chondrites. (a) the oxygen three-isotope diagram. The area highlighted by the dotted box is shown in the enlarged view. Reference lines are the same as those in Figure 4. (b) $\Delta^{17}O$ values of chondrules plotting in (a). The horizontal blue line represents the median value of all chondrules ($\Delta^{17}O = -5.2$). Error bars are 2σ. Literature data obtained with SIMS (CV SIMS) are from [1] Rudraswami et al. (2011), [2] Hertwig et al. (2018), [3] Hertwig, Kimura, Defouilloy, et al. (2019). (Color figure can be viewed at wileyonlinelibrary.com)

olivine and pyroxene analyses as the uncertainty of mean O isotope ratios instead of the calculation procedure described in Material S1.

Mean chondrule O isotope ratios of the five chondrules are listed in Table 1 and plotted in Figure 5a. Chondrule AL1 and AL4 plot at the high-end of the cluster of the literature data and between the Primitive Chondrule Minerals (PCM; Ushikubo et al., 2012) and Carbonaceous Chondrite Anhydrous Mineral (CCAM; Clayton et al., 1977) lines. Al-rich chondrule AL3 is significantly enriched in ^{16}O compared with the majority of CV chondrules. In contrast, the other chondrule AL2 and AL5 are depleted in ^{16}O and plot on the terrestrial fractionation (TF; Clayton et al., 1991) line.

Chromium and Titanium Isotope Ratios

The Cr and Ti isotope ratios of the three chondrules (AL1, AL2, AL3) are listed in Table 2, and their $\varepsilon^{54}Cr$ and $\varepsilon^{50}Ti$ values are plotted in Figure 6a. In a Cr-Ti isotope diagram, two chondrules (AL1 and AL3) are plotted within the bulk CC meteorite space (Figure 6a). The other chondrule AL2 exhibits both CC- and NC-like isotopic signatures. For this chondrule AL2, the $\varepsilon^{54}Cr$ value is 0.6 ± 0.1 (2σ), which is within the range of bulk CC meteorites. In contrast, chondrule AL2 exhibits a negative $\varepsilon^{50}Ti$ value of -0.7 ± 0.4 (2σ), which is rather consistent with those of bulk NC meteorites.

DISCUSSION

The Effect of Parent Body Processes on the Cr-Ti-O Isotope Systematics

As observed in previous studies (Schneider et al., 2020; Williams et al., 2020), we find large variations in (Cr)-Ti-O isotope ratios of Allende chondrules, which could provide constraints on the early disk dynamics. The CV carbonaceous chondrites, including Allende, possess evidence for various degrees of aqueous alteration, thermal metamorphism, and metasomatism (e.g., Brearley & Krot, 2013; Krot et al., 1998). These post-accretion processes might have modified the primary Cr-Ti-O isotope systematics of CV chondrules, resulting in the observed isotopic variations. Here, we discuss the possible effects on the Cr-Ti-O isotope systematics during post-accretion processes.

Oxygen isotope systematics could be influenced by parent body processes. Jabeen et al. (2019) measured bulk O isotope ratios of 32 Allende chondrules using laser-assisted fluorination mass spectrometry and pointed out that bulk O isotope ratios of Allende chondrules would be modified by aqueous alteration on the parent body based on a steeper slope for their measured chondrules compared with the slope ~1 in the oxygen three-isotope diagram. However, all O isotope data discussed here are obtained with in situ SIMS olivine and pyroxene analyses

TABLE 2. Titanium and chromium isotope ratios of three chondrules from Allende (CV3.6) carbonaceous chondrite.

Chondrule	Type	ε^{46}Ti	Unc.[a]	ε^{48}Ti	Unc.[a]	ε^{50}Ti	Unc.[a]	ε^{53}Cr	Unc.[a]	ε^{54}Cr	Unc.[a]
AL1	Type I, BO	0.76	0.33	0.16	0.10	4.30	0.26	0.07	0.04	0.64	0.11
AL2	Type I, BO	−0.27	0.30	0.05	0.10	−0.71	0.35	−0.03	0.07	0.63	0.11
AL3	Al-rich	0.41	0.23	−0.70	0.07	2.24	0.19	0.12	0.07	1.07	0.08

[a]Quoted uncertainties are at 2σ level.

that could avoid altered phases such as plagioclase and glassy mesostases. Oxygen isotope ratios of olivine and pyroxene grains in Allende and Karoonda chondrules seem to be consistent with those in more pristine CV chondrites Kaba and NWA 8613 (Hertwig et al., 2018; Hertwig, Kimura, Defouilloy, et al., 2019; Williams et al., 2020), supporting that olivine and pyroxene grains preserve their primary O isotope signatures even for the equilibrated chondrite Karoonda (CK4).

The effect of post-accretion processes on Cr and, perhaps, Ti isotopes could be more tricky. van Kooten et al. (2021) investigated relationships in Cr isotope ratios between chondrule cores and igneous rims from Leoville (CV3.1-3.4; Bonal et al., 2006), which is one of the least altered CV chondrites. The ε^{54}Cr values of the Leoville chondrule cores define a relatively narrow range ($-1.0 \leq \varepsilon^{54}\text{Cr} \leq -0.1$; except for two Al-rich chondrules) and are systematically lower than those of their corresponding igneous rims and those of chondrules from possibly more metamorphosed CV chondrites, such as Vigarano (CV3.1–3.4; Bonal et al., 2006; but could be more metamorphosed as ~3.6; Righter et al., 2023), Northwest Africa (NWA) 3118 (CV3; Russell et al., 2005), and Allende (CV3.6; Bonal et al., 2006) (Figure 7). On this basis, van Kooten et al. (2021) proposed that Cr isotope systematics of chondrules from Vigarano, NWA 3118, and Allende have been modified by parent body processes, that is, isotopic exchange between chondrules and matrix materials (± surrounding igneous rims). Here, we raise some issues with this interpretation by comparing CV3 chondrule data to those from Karoonda (CK4). A genetic relationship between CV and CK chondrites has been proposed based on similarities between the two groups (Weisberg et al., 2006). Several studies suggested that they form a continuous metamorphic series deriving from a single parent body (Chaumard et al., 2014; Chaumard & Devouard, 2016; Davidson et al., 2014; Greenwood et al., 2010; Wasson et al., 2013), though other studies disagree (Dunn et al., 2016, 2018; Yin & Sanborn, 2019). Nevertheless, CK4 chondrites experienced parent body thermal metamorphism at higher degrees than those for CV3 chondrites. If the interpretation by van Kooten et al. (2021) is correct, Karoonda chondrules would exhibit homogeneously positive ε^{54}Cr values similar to the bulk CK chondrite, though they show a significant range of ε^{54}Cr values similar to those of CV3 chondrules (Figure 7; Olsen et al., 2016; Williams et al., 2020). Furthermore, ε^{54}Cr values of Karoonda chondrules are often coupled with their ε^{50}Ti and Δ^{17}O values. For instance, Karoonda chondrules with positive ε^{54}Cr values exhibit positive ε^{50}Ti values (Figure 6a), of which Δ^{17}O values are similar to those in typical CC chondrules. If all Karoonda chondrules originally had NC-like isotopic compositions, and their primary isotopic compositions were modified by thermal metamorphism toward CC-like isotopic compositions, the observed coupling requires isotope exchange for all Cr, Ti, and O isotopes. However, as mentioned above, oxygen isotope ratios of olivine grains in Karoonda chondrules seem to preserve their primary O isotope signatures. Thus, the observed coupling among Cr-Ti-O isotope systematics is challenging to be explained solely by post-accretion processes. As for Cr isotopes, Ti and O isotope variability in Karoonda chondrules are similar to those of chondrules in less metamorphosed Allende (Figure 6a–c), supporting that both Cr and Ti in the bulk chondrules and olivine O isotopes retain their primary signatures even with the more metamorphosed Karronda CK4 chondrules (Williams et al., 2020). On the basis of these arguments, the correlated Cr-Ti-O isotope variations in the CK and CV chondrules studied so far seem to largely result from their various formation conditions/environments in the protoplanetary disk.

Note, however, that some chondrules could have potentially experienced minor Cr isotope exchange during the thermal metamorphism (van Kooten et al., 2021). The major carriers of Cr and Ti in chondrules are not the same mineral phases: that is, Cr could be in both olivine and pyroxene, whereas Ti is dominantly in pyroxene. Within the range of peak metamorphic temperatures for CV and CK chondrites (850 K < T < 1140 K; for example, Chaumard & Devouard, 2016), Ti-diffusion rate in pyroxene would be ~1–6 orders of magnitude smaller than Cr-diffusion rate in Mg-rich olivine (Mg# > 90) (e.g., Cherniak & Liang, 2012; Ito & Ganguly, 2006; Jollands et al., 2018; Spandler & O'Neill, 2009). Note that Ti-diffusion in pyroxene is very slow (Cherniak & Liang, 2012). Specifically, a Ti-diffusion distance of

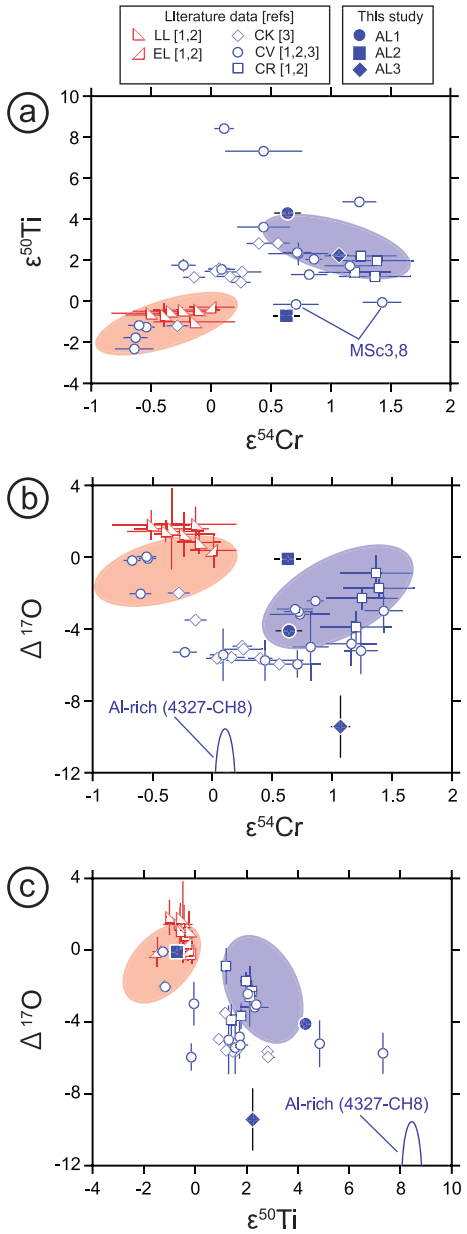

FIGURE 6. The Cr-Ti-O systematics of chondrules. (a) ε^{50}Ti versus ε^{54}Cr, (b)Δ^{17}O versus ε^{54}Cr, and (c) Δ^{17}O versus ε^{50}Ti. For (a–c), the ranges of bulk non-carbonaceous and carbonaceous meteorite groups are shown as red and blue fields, respectively, which are based on data compiled by Burkhardt et al. (2019) and data from Williams et al. (2020). Data from [1] Schneider et al. (2020), [2] Gerber et al. (2017), and [3] Williams et al. (2020). (Color figure can be viewed at wileyonlinelibrary.com)

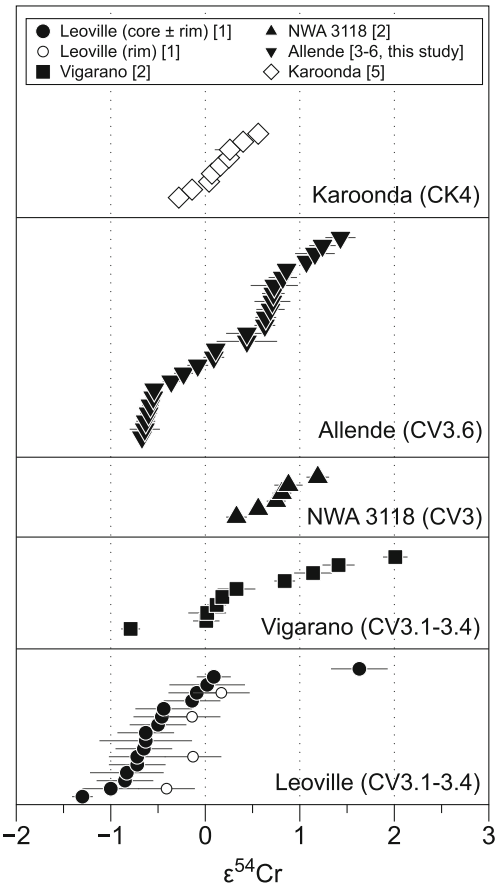

FIGURE 7. Compilation of ε^{54}Cr values of individual chondrules from CV and CK chondrites. Literature data from [1] van Kooten et al. (2021), [2] Olsen et al. (2016), [3] Trinquier et al. (2007), [4] Connelly et al. (2012), [5] Williams et al. (2020), [6] Schneider et al. (2020).

100 μm requires more than 10^{10} years at a peak metamorphic temperature of ~920 K estimated for CK4s (Geiger & Bischoff, 1991), which is far longer than the probable time scale of metamorphism. If the Cr isotope variation is of a metamorphic origin, therefore, a decoupling of Cr and Ti isotope signatures (i.e., NC-like Ti and CC-like Cr isotope signatures) is expected among chondrules in chondrites, for which metamorphic degrees are lower than CK4. In fact, three of the Allende chondrules (AL2 [this study], MSc3, and MSc8; Gerber et al., 2017; Schneider et al., 2020) exhibit these signatures, meaning that these chondrules could have potentially experienced minor Cr isotope exchange during the thermal metamorphism. Their NC-like negative ε^{50}Ti values but CC-like positive ε^{54}Cr values (Figure 6a) would be explained by the Cr isotope exchange between chondrules and matrix (ε^{54}Cr = 1.06 ± 0.22; Schneider et al., 2020) without Ti isotope modification. Regarding AL2, therefore, the possible effects of secondary alteration on Cr isotopes cannot be ruled out.

Altogether, we suggest that the observed Cr-Ti-O isotope variations in major CV and CK chondrules analyzed so far primarily result not from secondary alteration on the parent bodies but from their various formation conditions/environments in the protoplanetary disk. However, the Cr isotope system of some chondrules

(e.g., AL2, MSc3, and MSc8) could potentially be disturbed by thermal metamorphism on the parent body. Further studies of pristine chondrules are required to distinguish the primary or secondary origin of the CC-like Cr isotope signature.

Outward Transport of Chondrules and CAIs and Their Nebular Thermal Reprocessing in the Outer Solar System

The relationships between petrographic and in situ O isotopic characteristics, as well as Cr-Ti-O isotope systematics, provide important information about chondrule-forming environments, solid transport, and reprocessing in the protoplanetary disk. Here, we discuss formation scenarios of two chondrules, AL2 and AL3, showing O isotope disequilibrium among coexisting minerals, which are likely caused by multiple nebular thermal processing in the inner and outer regions of the Solar protoplanetary disk.

The BO chondrule AL2 (Mg# = 98) exhibits unique O isotope systematics between the olivine core and pyroxene igneous rim. The olivine core is obviously ^{16}O-depleted ($\Delta^{17}O = -0.1 \pm 0.2‰$; 2SD) compared with typical type I chondrules from CV chondrites (median $\Delta^{17}O = -5.2‰$; Figure 5a). The ^{16}O-depleted signature is consistent with an O isotope characteristic of chondrules originating from the inner Solar System (Kita et al., 2010; Miller et al., 2017; Nagashima et al., 2015; Piralla et al., 2021; Schrader et al., 2020; Siron et al., 2021, 2022; Weisberg et al., 2011, 2021). In contrast, the pyroxene igneous rim of chondrule AL2 is significantly enriched in ^{16}O ($\Delta^{17}O = -4.6 \pm 0.3‰$; 2SD) compared with the olivine core, which is rather consistent with typical type I chondrules from CV chondrites. In detail, olivine analyses plot above the PCM line, while those of the pyroxene igneous rim plot below the PCM line (Figure 4d). Previous studies revealed the presence of chondrules with ^{16}O-depleted, NC-like O isotope signatures in carbonaceous chondrites, suggesting that these chondrules and/or their precursors formed in the inner Solar System and were migrated toward the outer Solar System (Hertwig, Kimura, Defouilloy, et al., 2019; Schrader et al., 2020; Tenner et al., 2017). Williams et al. (2020) found that O isotope ratios of CV and CK chondrules with negative ε^{54}Cr (i.e., NC-like values) plot above the PCM line, while those with positive ε^{54}Cr values (i.e., CC-like values) plot below the PCM line. On this basis, Williams et al. (2020) proposed that the former and latter originated from the inner and outer Solar System, respectively. Thus, the O isotope systematics of chondrule AL2 may suggest that the formation of the olivine core and pyroxene igneous rim took place in the inner and outer Solar System, respectively. This hypothesis is consistent with the NC-like negative ε^{50}Ti value recorded in the olivine core (Figure 6c). However, the ε^{54}Cr value recorded in the olivine core is rather consistent with carbonaceous chondritic materials, which would have resulted from isotope exchange during nebular thermal reprocessing that originated the pyroxene igneous rim in the outer Solar System. Since olivine appears to have partially melted during the igneous rim formation (Figure 2c,d), the temperature of the nebular thermal processing would be near the solidus temperature of olivine (>2100 K for forsterite). In this temperature range, the Cr-diffusion rate in Mg-rich olivine (Mg# > 90) is ~1–5 orders of magnitude larger than the O-diffusion rate in olivine and the Ti-diffusion rate in pyroxene (e.g., Ando et al., 1981; Cherniak & Liang, 2012; Ito & Ganguly, 2006; Jaoul et al., 1980; Jollands et al., 2018). Accordingly, isotope exchange could occur only for Cr between olivine and melt during the nebular thermal processing, but not for O in olivine and Ti in pyroxene in the core. Alternatively, mesostasis could also be a carrier of Cr in the core. Isotope exchange between surrounding gas and chondrule melt that eventually generates mesostasis would occur by gas–melt interaction during the nebular thermal processing. The surrounding gas would not contain too much Ti, but Cr due to the difference in their volatilities. In this case, it is possible that mesostasis acquires CC-like Cr, but would maintain NC-like Ti isotope signatures. It should be noted, however, that the possible secondary origin of the CC-like Cr isotope signature in the core cannot be ruled out (van Kooten et al., 2021; see the previous section). Regardless of the origin of CC-like Cr isotope signature, the petrography, in situ O isotope systematics, and Ti-O isotope systematics of chondrule AL2 provide further evidence for outward transport of chondrules/fragments from the inner Solar System (Schrader et al., 2020; Tenner et al., 2017; van Kooten et al., 2021; Williams et al., 2020) and its subsequent nebular thermal reprocessing in the outer Solar System.

The Al-rich chondrule AL3 exhibits significant O isotope heterogeneity among coexisting minerals (Figure 4e). Plagioclase grains are systematically depleted in ^{16}O compared with olivine and pyroxene (Figure 4e), which is often observed in chondrules from aqueously and thermally altered CV chondrites (Akaki et al., 2007; Chaussidon et al., 2008; Hertwig, Kimura, Defouilloy, et al., 2019; Krot & Nagashima, 2016; Maruyama et al., 1999; Maruyama & Yurimoto, 2003; Rudraswami et al., 2011; Wakaki et al., 2013; Zhang et al., 2020). Since the O-diffusion rate in plagioclase is larger than those in olivine and pyroxene (Giletti et al., 1978; Ryerson & McKeegan, 1994), it is conceivable that plagioclase grains experienced O isotope exchange with ^{16}O-depleted metasomatic fluid on the CV parent body (Hertwig, Kimura, Defouilloy, et al., 2019; Krot et al., 2019). Thus, we do not use O isotope data of plagioclase grains to

argue a formation scenario of chondrule AL3, as discussed below. Regarding spinel grains in chondrule AL3, their extremely ^{16}O-rich characteristics (Figure 4e,f) and corroded textures (Figure 3c) suggest that they are relict of a ^{16}O-rich refractory precursor material, which could have survived the nebular thermal processing that crystallized olivine and pyroxene grains from the chondrule melt. In addition to the refractory precursor, a ^{16}O-depleted, less-refractory precursor is required to explain the presence of ^{16}O-depleted olivine and pyroxene grains compared with spinel grains (Figure 4e). These observations suggest that this chondrule formed by incomplete melting of solid precursors composed of ^{16}O-rich refractory and ^{16}O-depleted less-refractory materials, consistent with the conclusions for the origin of other Al-rich chondrules (Krot et al., 2002, 2004; Krot & Keil, 2002; MacPherson & Huss, 2005; Sheng et al., 1991; Wakaki et al., 2013; Zhang et al., 2020). Importantly, O isotope ratios of olivine and pyroxene grains plot between the PCM and CCAM lines (Figure 4g), while those of spinel grains plot on the PCM line (Figure 4f). The former is a common characteristic of chondrules from the majority of CV chondrites as well as CO and CM (Chaumard et al., 2018, 2021; Fukuda et al., 2022; Hertwig et al., 2018; Hertwig, Kimura, Defouilloy, et al., 2019; Schrader et al., 2020; Tenner et al., 2013; Zhang et al., 2022), while the latter is consistent with O isotope characteristics of CAIs and amoeboid olivine aggregates (AOAs) from the least metamorphosed chondrites (e.g., Fukuda et al., 2021; Hiyagon & Hashimoto, 1999; Kööp et al., 2016; Krot et al., 2019; Ushikubo et al., 2017). On the basis of these observations, the formation scenario of chondrule AL3 can be inferred as follows: (i) the refractory precursor of chondrule AL3 formed in an environment where CAIs and AOAs formed, which is most likely the innermost region of the Solar protoplanetary disk (<1 AU; e.g., Shu et al., 1996; Wood, 2004), (ii) the ^{16}O-rich refractory precursor was transported to the outer Solar System and then experienced incomplete melting with the ^{16}O-depleted less-refractory precursor, which is most likely chondrules or related material generated in the outer Solar System.

In order to test this hypothesis, we calculated two-component mixing curves between ^{16}O-rich CV CAI-like and ^{16}O-depleted CV chondrule-like materials (Figure 8a–c; see also Material S1 for details of the calculation). The ε^{54}Cr-Δ^{17}O relationship of chondrule AL3 can be explained by a mixture between (20%) CV CAI-like and (80%) CV chondrule-like material (Figure 8b). If we consider large variations in Ti isotope ratios of CV CAIs as observed in several studies ($1 \leq \varepsilon^{50}\text{Ti} \leq 16$; e.g., Davis et al., 2018; Leya et al., 2009; Niederer et al., 1981; Render et al., 2019; Shollenberger et al., 2022; Simon et al., 2017; Torrano et al., 2023; Trinquier et al., 2009; Williams et al., 2016 and references therein), the ε^{54}Cr-ε^{50}Ti and ε^{50}Ti-Δ^{17}O relationships can also be explained by the mixture of CV CAI-like material with $\varepsilon^{50}\text{Ti} = 2$ and CV chondrule-like material (Figure 8a,c). Together, the Cr-Ti-O isotope systematics of chondrule AL3 are well explained by CAI transport and subsequent nebular thermal reprocessing in the outer Solar System, which is consistent with the observations of relict CAIs inside chondrules found in carbonaceous chondrites (e.g., Krot et al., 2002, 2004; Krot & Keil, 2002). Note that two other Al-rich chondrules that have been previously investigated for Cr-Ti-O isotope systematics cannot be explained by nebular thermal processing of the mixture of CV CAI-like and CV chondrule-like material (Figure 8a–c), which would require an alternative ^{16}O-depleted component, such as NC-like material (Figure 8d–f; Schneider et al., 2020; Williams et al., 2020). Regarding one of the Al-rich chondrule 4327-CH8 studied by Williams et al. (2020), O isotope ratios of olivine and pyroxene plot on or marginally above the PCM line, although most of which cannot be resolved from the PCM line beyond their uncertainties. This is consistent with its formation by nebular thermal processing of the mixture of CAI and NC-like materials (Figure 8d–f), meaning that this chondrule or at least one of its precursors formed in the inner Solar System (Williams et al., 2020). Altogether, these Al-rich chondrules have formed by incomplete melting of various solid precursors, including CAIs, CC-like, and NC-like materials originating from various regions in the Solar protoplanetary disk.

Larger Chondrules may have Distinct Isotopic Signatures

Five chondrules studied here do not have typical O isotope ratios of the majority of MgO-rich (Mg# > 90) CV chondrules with Δ^{17}O from −6‰ to −4‰ (median = −5.2‰; Figure 5b; Hertwig et al., 2018; Hertwig, Kimura, Defouilloy, et al., 2019; Rudraswami et al., 2011). This could reflect a sampling bias as we selected relatively larger chondrules (>1.5 mm in diameter) compared with typical CV chondrules (~0.9 mm in diameter; Friedrich et al., 2015), in order to obtain high-precision Cr-Ti isotope data. Figure 9 compiled ε^{54}Cr, ε^{50}Ti, and Δ^{17}O values of CV chondrules as a function of their mean sizes (Connelly et al., 2012; Gerber et al., 2017; Hertwig et al., 2018; Hertwig, Kimura, Defouilloy, et al., 2019; Olsen et al., 2016; Rudraswami et al., 2011; Schneider et al., 2020; Trinquier et al., 2009; Williams et al., 2020; this study; Note that Leoville chondrules in van Kooten et al. (2021) are not included in this figure due to the lack of size information). It can be clearly seen that the chondrules studied for combined Cr-Ti-O isotope systematics so far are larger than the average size of CV chondrules (~0.9 mm). Importantly, the ε^{54}Cr values of some larger CV chondrules do not distribute along the average ε^{54}Cr

value of pooled Allende chondrules (0.91 ± 0.12, 2σ; Kadlag et al., 2019), and tend to have lower ε^{54}Cr values relative to the average ε^{54}Cr value (Figure 9a).

The relationships between Δ^{17}O-ε^{50}Ti values and chondrule sizes seem more complex (Figure 9b,c). This could arise from the fact that CV chondrules formed from various precursor materials with distinct Ti and O isotope ratios (i.e., refractory inclusions, NC-like, and CC-like materials), as discussed above. In particular, Ti isotope ratios of CAIs are quite variable compared with other Solar System objects (e.g., Davis et al., 2018; Kööp et al., 2016; Leya et al., 2009; Render et al., 2019; Trinquier et al., 2009; Williams et al., 2016). Further, Ti concentrations of CAIs are ~1–3 orders of magnitude higher than chondrules. Thus, the incorporation of small amounts of CAI-like material results in a significant shift of Ti isotope ratios of generated chondrules, while this is not the case for Cr due to its depletion in CAIs. The majority of CAIs in pristine CV carbonaceous chondrites also exhibit ^{16}O-rich isotopic characteristics (e.g., Krot, 2019; Ushikubo et al., 2017). If chondrule precursors contain substantial amounts of CAIs, therefore, the generated chondrules would be enriched in ^{16}O, as evidenced by Al-rich chondrules (Figure 9c). The incorporation of CAI-like material may explain why Ti and O isotope data do not show clear trends against chondrule sizes.

Note that larger chondrules, except for two Al-rich chondrules, tend to have relatively ^{16}O-depleted characteristics (Δ^{17}O > −5‰; Figure 9c), which is distinct from the majority of smaller chondrules. Similarly, negative ε^{50}Ti as well as ε^{54}Cr values are often observed among larger chondrules (Figure 9a,b). These observations indicate that some larger chondrules in CV chondrites or their precursors formed in distinct disk environments, which are most likely the inner Solar System. Again, the majority of CV chondrules studied for Cr and Ti isotope systematics are obviously larger than the typical size of CV chondrules (~0.9 mm) (Figure 9; Connelly et al., 2012; Olsen et al., 2016; Schneider et al., 2020; Williams et al., 2020; this study), which may not be representative of the typical CV chondrule population. Therefore, it would not be an appropriate way to discuss the population of NC-like chondrules in carbonaceous chondrites based only on the present data set. Further, Cr-Ti-O isotope studies on individual chondrules with a more typical size (~0.9 mm) are needed to assess the efficiency of outward transport during the lifetime of the Solar protoplanetary disk.

Implications for Dynamics in the Solar Protoplanetary Disk

By combining the results from previous studies, we showed that some CV chondrules larger than 1.5 mm diameter exhibit NC-like Cr-Ti-O isotope signatures, which sheds light on the early disk dynamics. As mentioned in the introduction, the presence of a physical barrier is required to maintain isotope dichotomy between the inner and outer Solar System, which would have significantly hindered the mixing and transport of materials from one to another (Desch et al., 2018; Kleine et al., 2020; Kruijer et al., 2017). However, the presence of NC chondrite-like chondrules/fragments in carbonaceous chondrites suggests that the outward transport of inner Solar System materials is far more frequent (Schrader et al., 2020; van Kooten et al., 2021; Williams et al., 2020). It is inferred, therefore, that the physical barrier has not completely prohibited the outward transport of inner Solar System materials, consistent with the temporal change of Ca and Fe isotope ratios of inner Solar System bodies toward CC-like isotope signatures throughout the disk's lifetime (Schiller et al., 2018, 2020).

Although the origin of the physical barrier is actively debated, one of the plausible candidates is the formation of a proto-Jupiter or related disk gap (Jupiter gap, Brasser & Mojzsis, 2020; Kruijer et al., 2017). Numerical modeling combined with observed sizes of CAIs in NC chondrites suggest smaller materials (<300 μm) could have passed through the physical barrier (Haugbølle et al., 2019), which is consistent with the observation that ^{16}O-depleted relict grains (Δ^{17}O ~ 0‰) found in some carbonaceous chondrite chondrules are smaller than ~400 μm diameter (Schrader et al., 2020). However, it seems unlikely that NC chondrite chondrules larger than 1.5 mm diameter could have passed through the Jupiter gap since larger grains are concentrated in a local maximum in the gas pressure due to friction forces between gas and grains (Whipple, 1972), although a threshold of grain size passing through the Jupiter gap would depend on several disk parameters, such as level of disk turbulence (e.g., Desch et al., 2018; Weber et al., 2018). Therefore, the presence of large NC chondrite-like chondrules in carbonaceous chondrites would require that outward migration of these chondrules have occurred before the creation of the Jupiter gap (Hellmann et al., 2023). The Mo isotope systematics and Hf-W model ages of iron meteorites suggest that the proto-Jupiter formed between the NC and CC reservoirs within ~1 Ma after CAI formation (Kruijer et al., 2017; Spitzer et al., 2021). In this case, migration of NC chondrite chondrules must have been completed before ~1 Ma after CAI formation. However, the majority of chondrules from NC chondrites, unequilibrated ordinary chondrites (UOCs), formed >1.8 Ma after CAIs (e.g., Kita et al., 2000; Pape et al., 2019; Siron et al., 2021, 2022; Villeneuve et al., 2009), which may not support the early (<1 Ma after CAIs) outward migration of NC chondrite chondrules into carbonaceous chondrite accretion regions.

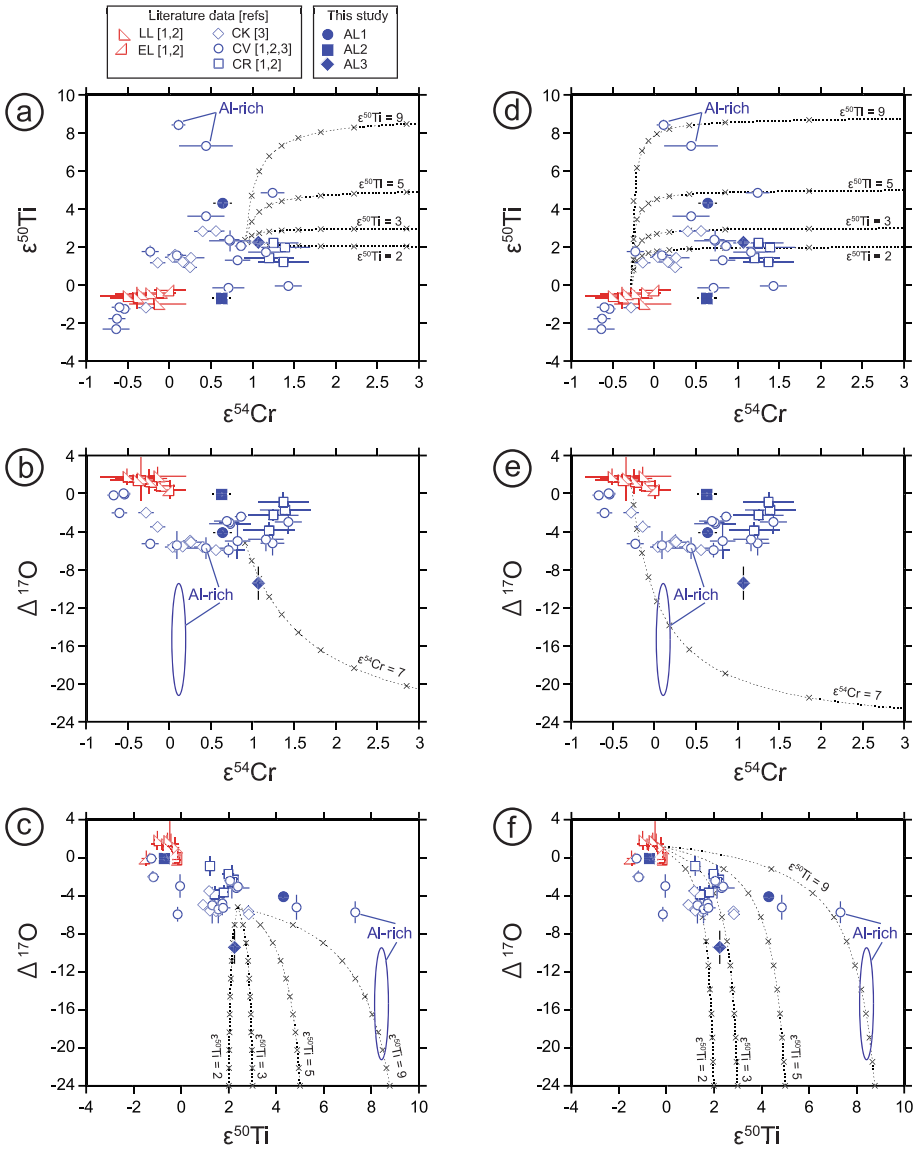

FIGURE 8. The Cr-Ti-O systematics of chondrules and their comparisons with two-component mixing models. (a, d) ε^{50}Ti versus ε^{54}Cr, (b, e)Δ^{17}O versus ε^{54}Cr, and (c, f) Δ^{17}O versus ε^{50}Ti. The calculated mixing trends for *Model 1* (mixing between CV chondrules and CV CAIs with variable Ti isotope ratios) and *Model 2* (mixing between ordinary chondrite (OC) chondrules and CV CAIs with variable Ti isotope ratios) are also shown in (a–c) and (d–f), respectively (see Material S1 for more details of mixing calculations). The Al-rich chondrule 4327-CH8 studied by Williams et al. (2020) exhibits heterogeneous oxygen isotope ratios ($-20.1 < \Delta^{17}O < -10.0$) and is therefore displayed as a blue ellipse covering the entire range. Crosses on mixing lines indicate a 10% addition of CAI components into CV chondrules or OC chondrules. The Cr-Ti-O isotope systematics of Al-rich chondrule AL3 can be explained by *Model 1*, in which the CAI component has ε^{50}Ti = 2. Note that the two mixing models cannot reproduce all chondrules as shown here, which require additional/alternative endmembers, such as AOA-like material (see Schneider et al., 2020; Williams et al., 2020). Data from [1] Schneider et al. (2020), [2] Gerber et al. (2017), and [3] Williams et al. (2020). (Color figure can be viewed at wileyonlinelibrary.com)

Hertwig, Kimura, Ushikubo, et al. (2019) argued that the two ^{16}O-depleted, NC-like chondrules G39 and G85 in Acfer 094 formed in the inner Solar System and then were migrated toward the outer Solar System at >1.6 Ma after CAIs based on their Al-Mg ages (1.79 $^{-0.16}/_{+0.19}$ Ma and 1.75 $^{-0.11}/_{+0.12}$ Ma after CAIs, respectively, the former of which was determined by Ushikubo et al., 2013).

Note that the formation ages of UOC chondrules have been determined mostly by in situ Al-Mg analyses of chondrule plagioclase or glassy mesostases, which should represent the time of the last melting events generating UOC chondrules. Therefore, it is also possible that UOC chondrule formation might have taken place earlier than ~1.8 Ma after CAIs, as suggested by Pb-Pb and Al-Mg

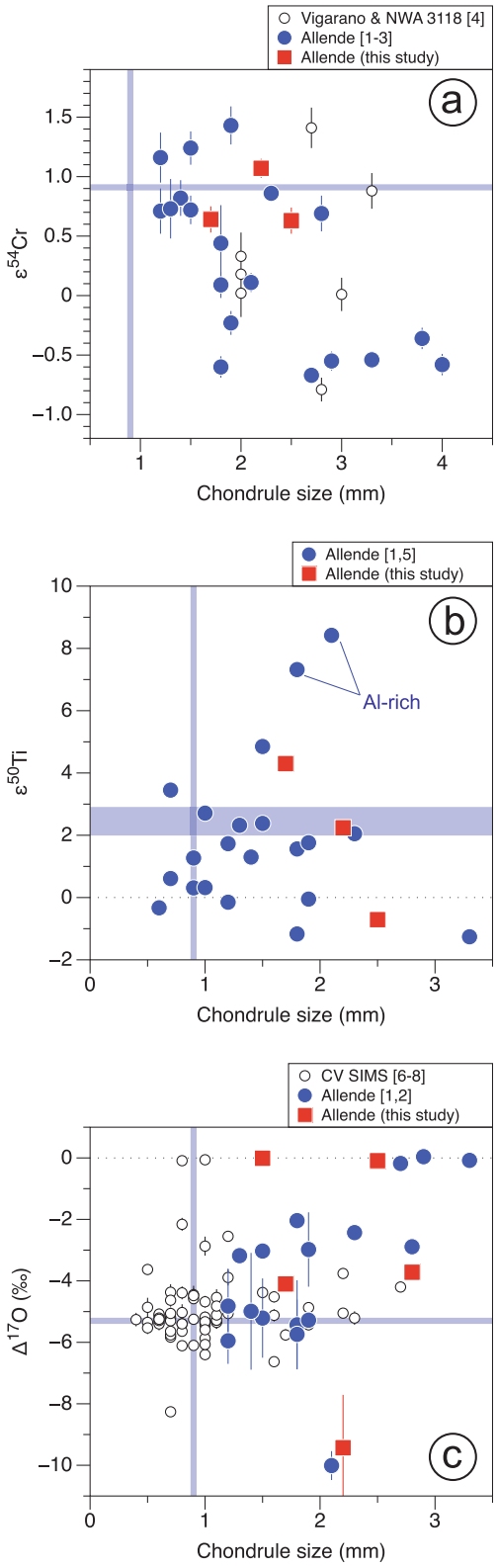

FIGURE 9. ε^{54}Cr, ε^{50}Ti, and Δ^{17}O values as a function of chondrule sizes for CV chondrules. For (a–c), the vertical line (blue) represents an average chondrule size of CV chondrules (0.9 mm diameter; Friedrich et al., 2015). For (b, c), Chondrule sizes of literature data are compiled in Table S6, which are from reported values (Gerber et al., 2017) or are determined from backscattered electron images of individual chondrules if available. (a) ε^{54}Cr versus chondrule sizes. The horizontal line (blue) represents the ε^{54}Cr value of pooled Allende chondrules (ε^{54}Cr = 0.91; Kadlag et al., 2019). (b) ε^{50}Ti versus chondrule sizes. The horizontal field (blue) represents the range of ε^{50}Ti values of pooled Allende chondrules ($2.0 < \varepsilon^{50}\text{Ti} < 2.9$; Gerber et al., 2017). Two Al-rich chondrules from Williams et al. (2020) and Schneider et al. (2020) are indicated. (c) Δ^{17}O versus chondrule sizes. The horizontal line (blue) represents the median Δ^{17}O value for CV chondrules ($\Delta^{17}\text{O} = -5.2‰$; Hertwig et al., 2018; Hertwig, Kimura, Defouilloy, et al. (2019); Rudraswami et al., 2011; this study). Two Al-rich chondrules from Williams et al. (2020) and this study (AL3) are indicated. Error bars are 2σ. Literature isotope data from [1] Williams et al. (2020), [2] Schneider et al. (2020), [3] Connelly et al. (2012), [4] Olsen et al. (2016), [5] Gerber et al. (2017), [6] Rudraswami et al. (2011), [7] Hertwig et al. (2018), and [8] Hertwig, Kimura, Defouilloy, et al. (2019). (Color figure can be viewed at wileyonlinelibrary.com)

dating (Bollard et al., 2017; Connelly et al., 2012; Piralla et al., 2023). In this case, three possible scenarios can be considered to explain why the majority of UOC chondrules older than 1.8 Ma after CAIs are almost absent. First, the earlier generation of UOC chondrules may have been accreted into early-formed planetesimals in the inner Solar System. Planetesimals that accreted during the first 1.5 Ma after CAIs would have fully melted by the decay energy of ^{26}Al (e.g., Sanders & Scott, 2012) so that the accretion of chondrules into these planetesimals would not allow survival of the earlier generation of UOC chondrules. Second, later chondrule-forming events may have recycled the earlier generation of UOC chondrules. As discussed by Rubin (2010), many chondrules appear to have been melted more than once, as evidenced by the presence of chemically and isotopically relict grains (e.g., Jones, 1996; Krot et al., 2006; Marrocchi et al., 2018, 2019; Nagahara, 1981; Rambaldi, 1981; Tenner et al., 2013; Ushikubo et al., 2012; Wasson & Rubin, 2003; Yurimoto & Wasson, 2002), the presence of enveloping compound chondrules such as AL1 (Figure 1a; Wasson et al., 1995), igneous rims around chondrule core such as AL2 (Figure 2a) (e.g., Krot & Wasson, 1995; Rubin, 1984, 2010), and the presence of lobate chondrules (Jacquet, 2021; Rubin & Wasson, 2005). Third, the earlier generation of UOC chondrules may have been transported outwards (and inwards) from their formation regions before the creation of the Jupiter gap. This hypothesis could be tested by determining the Al-Mg ages of chondrules with NC-like Cr-Ti-O isotope signatures in carbonaceous chondrites. Up to now, such chondrules are only found in thermally metamorphosed

carbonaceous chondrites Allende (CV3.6) and Karoonda (CK4) (Williams et al., 2020). Al-Mg systematics of chondrule plagioclase and glassy mesostases in thermally metamorphosed chondrites were often disturbed (Nagashima et al., 2017; Sano et al., 2014), which do not allow for determining Al-Mg ages of Allende and Karoonda chondrules. Future combined Al-Mg and Cr-Ti-O isotope systematics of chondrules from pristine carbonaceous chondrites will reveal time scales of outward transport from the inner Solar System.

CONCLUSIONS

Our petrography and combined Cr-Ti-O isotope systematics of chondrules provide further evidence for the outward transport of CAIs and chondrules from the inner to the outer region of the protoplanetary disk. Some of the transported CAIs and chondrules are consumed as one of the precursors to forming CC chondrules. By combining the previously reported data set, we find larger (>1.5 mm) CV chondrules tend to have distinct, NC-like isotope signatures, indicating outward migration of NC-like materials from the inner disk to the CV chondrule-forming region. This outward migration of mm-sized solids should have occurred within ~1 Ma after CAI formation (i.e., the creation of Jupiter gap) since the limited transport of mm-sized grains between the inner and the outer Solar System is expected due to the development of Jupiter gap. Yet, combined Cr-Ti-O and Al-Mg investigations on pristine chondrules will be required to elucidate the timing of outward migration. Note that the chondrule Cr-Ti-O systematics investigated so far are largely determined from unusually large chondrules. Further, Cr-Ti-O isotope studies on individual chondrules of a more typical size are required to assess the efficiency of outward transport during the lifetime of the Solar protoplanetary disk.

Acknowledgments—We acknowledge Glenn MacPherson (National Museum of Natural History, Smithsonian Institution) for the allocation of the Allende sample for this study. We thank Brian Beard and Mike Tappa for helping us clean vials for sample digestion, Michael Spicuzza for SIMS support, Bil Schneider for help with SEM observations, and Drae Rogers for assistance with sample preparation. We are also grateful to Alexander N. Krot, Devin L. Schrader, and an anonymous reviewer for their constructive and educational comments and associate editor Marc Caffee for effective handling. This work is supported by the NASA Emerging Worlds Program (80NSSC21K0378, N.T.K), JSPS KAKENHI grant number 21KK0057, and the University of Wisconsin-Madison, Office of the Vice Chancellor for Research and Graduate Education with funding from the Wisconsin Alumni Research Foundation. The WiscSIMS laboratory is partly supported by the NSF Instrumentation and Facility Program (EAR-1658823, EAR-2004618).

Conflict of Interest Statement—The authors declare that they have no known competing financial interests or personal relationships that could have appeared to influence the work reported in this article.

Data Availability Statement—The data that support the findings of this study are available in the supplementary material of this article.

Editorial Handling—Dr. Marc W. Cafee

REFERENCES

Akaki, T., Nakamura, T., Noguchi, T., and Tsuchiyama, A. 2007. Multiple Formation of Chondrules in the Early Solar System: Chronology of a Compound Al-Rich Chondrule. *The Astrophysical Journal* 656: L29–L32.

Amelin, Y., Kaltenbach, A., Iizuka, T., Stirling, C. H., Ireland, T. R., Petaev, M., and Jacobsen, S. B. 2010. U-Pb Chronology of the Solar System's Oldest Solids with Variable $^{238}U/^{235}U$. *Earth and Planetary Science Letters* 300: 343–350.

Ando, K., Kurokawa, H., and Oishi, Y. 1981. Self-Diffusion Coefficient of Oxygen in Single-Crystal Forsterite. *Journal of the American Ceramic Society* 64: C30.

Bermingham, K. R., Füri, E., Lodders, K., and Marty, B. 2020. The NC-CC Isotope Dichotomy: Implications for the Chemical and Isotopic Evolution of the Early Solar System. *Space Science Reviews* 216: 133.

Bockelée-Morvan, D., Gautier, D., Hersant, F., Huré, J.-M., and Robert, F. 2002. Turbulent Radial Mixing in the Solar Nebula as the Source of Crystalline Silicates in Comets. *Astronomy and Astrophysics* 384: 1107–18.

Bollard, J., Connelly, J. N., Whitehouse, M. J., Pringle, E. A., Bonal, L., Jørgensen, J. K., Nordlund, Å., Moynier, F., and Bizzarro, M. 2017. Early Formation of Planetary Building Blocks Inferred from Pb Isotopic Ages of Chondrules. *Science Advances* 3: e1700407.

Bonal, L., Quirico, E., Bourot-Denise, M., and Montagnac, G. 2006. Determination of the Petrologic Type of CV3 Chondrites by Raman Spectroscopy of Included Organic Matter. *Geochimica et Cosmochimica Acta* 70: 1849–63.

Bouvier, A., and Wadhwa, M. 2010. The Age of the Solar System Redefined by the Oldest Pb-Pb Age of a Meteoritic Inclusion. *Nature Geoscience* 3: 637–641.

Brasser, R., and Mojzsis, S. J. 2020. The Partitioning of the Inner and Outer Solar System by a Structured Protoplanetary Disk. *Nature Astronomy* 4: 492–99.

Brearley, A. J., and Krot, A. N. 2013. Metasomatism in the Early Solar System: The Record from Chondritic Meteorites. In *Metasomatism and the Chemical Transformation of Rock*, 659–789. Berlin: Springer.

Brownlee, D. E., and Joswiak, D. J. 2017. Diversity of the Initial Rocky Planetary Building Materials at the Edge of

the Solar System. *Meteoritics & Planetary Science* 52: 471–78.

Budde, G., Burkhardt, C., Brennecka, G. A., Fischer-Gödde, M., Kruijer, T. S., and Kleine, T. 2016. Molybdenum Isotopic Evidence for the Origin of Chondrules and a Distinct Genetic Heritage of Carbonaceous and Non-Carbonaceous Meteorites. *Earth and Planetary Science Letters* 454: 293–303.

Burkhardt, C., Dauphas, N., Hans, U., Bourdon, B., and Kleine, T. 2019. Elemental and isotopic variability in solar system materials by mixing and processing of primordial disk reservoirs. *Geochimica et Cosmochimica Acta* 261: 145–170.

Charlier, B. L. A., Ginibre, C., Morgan, D., Nowell, G. M., Pearson, D. G., Davidson, J. P., and Ottley, C. J. 2006. Methods for the Microsampling and High-Precision Analysis of Strontium and Rubidium Isotopes at Single Crystal Scale for Petrological and Geochronological Applications. *Chemical Geology* 232: 114–133.

Chaumard, N., Defouilloy, C., Hertwig, A. T., and Kita, N. T. 2021. Oxygen Isotope Systematics of Chondrules in the Paris CM2 Chondrite: Indication for a Single Large Formation Region across Snow Line. *Geochimica et Cosmochimica Acta* 299: 199–218.

Chaumard, N., Defouilloy, C., and Kita, N. T. 2018. Oxygen Isotope Systematics of Chondrules in the Murchison CM2 chondrite and Implications for the CO-CM Relationship. *Geochimica et Cosmochimica Acta* 228: 220–242.

Chaumard, N., and Devouard, B. 2016. Chondrules in CK Carbonaceous Chondrites and Thermal History of the CV–CK Parent Body. *Meteoritics & Planetary Science* 51: 547–573.

Chaumard, N., Devouard, B., Bouvier, A., and Wadhwa, M. 2014. Metamorphosed Calcium-Aluminum-Rich Inclusions in CK Carbonaceous Chondrites. *Meteoritics & Planetary Science* 49: 419–452.

Chaussidon, M., Libourel, G., and Krot, A. N. 2008. Oxygen Isotopic Constraints on the Origin of Magnesian Chondrules and on the Gaseous Reservoirs in the Early Solar System. *Geochimica et Cosmochimica Acta* 72: 1924–38.

Cherniak, D. J., and Liang, Y. 2012. Ti Diffusion in Natural Pyroxene. *Geochimica et Cosmochimica Acta* 98: 31–47.

Ciesla, F. J. 2007. Outward Transport of High-Temperature Materials Around the Midplane of the Solar Nebula. *Science* 318: 613–15.

Clayton, R. N., Mayeda, T. K., Goswami, J. N., and Olsen, E. J. 1991. Oxygen Isotope Studies of Ordinary Chondrites. *Geochimica et Cosmochimica Acta* 55: 2317–37.

Clayton, R. N., Onuma, N., Grossman, L., and Mayeda, T. K. 1977. Distribution of the Pre-Solar Component in Allende and Other Carbonaceous Chondrites. *Earth and Planetary Science Letters* 34: 209–224.

Connelly, J. N., Bizzarro, M., Krot, A. N., Nordlund, Å., Wielandt, D., and Ivanova, M. A. 2012. The Absolute Chronology and Thermal Processing of Solids in the Solar Protoplanetary Disk. *Science* 338: 651–55.

Cuzzi, J. N., Hogan, R. C., and Bottke, W. F. 2010. Towards Initial Mass Functions for Asteroids and Kuiper Belt Objects. *Icarus* 208: 518–538.

Davidson, J., Krot, A. N., Nagashima, K., Hellebrand, E., and Lauretta, D. S. 2014. Oxygen Isotope and Chemical Compositions of Magnetite and Olivine in the Anomalous CK3 Watson 002 and Ungrouped Asuka-881595 Carbonaceous Chondrites: Effects of Parent Body Metamorphism. *Meteoritics & Planetary Science* 49: 1456–74.

Davis, A. M., Zhang, J., Greber, N. D., Hu, J., Tissot, F. L. H., and Dauphas, N. 2018. Titanium Isotopes and Rare Earth Patterns in CAIs: Evidence for Thermal Processing and Gas-Dust Decoupling in the Protoplanetary Disk. *Geochimica et Cosmochimica Acta* 221: 275–295.

Defouilloy, C., Nakashima, D., Joswiak, D. J., Brownlee, D. E., Tenner, T. J., and Kita, N. T. 2017. Origin of Crystalline Silicates from Comet 81P/Wild 2: Combined Study on their Oxygen Isotopes and Mineral Chemistry. *Earth and Planetary Science Letters* 465: 145–154.

Desch, S. J., Kalyaan, A., and Alexander, C. M. O. D. 2018. The Effect of Jupiter's Formation on the Distribution of Refractory Elements and Inclusions in Meteorites. *The Astrophysical Journal Supplement Series* 238: 11.

Dunn, T. L., Battifarano, O. K., Gross, J., and O'hara, E. J. 2018. Characterization of Matrix Material in Northwest Africa 5343: Weathering and Thermal Metamorphism of the Least Equilibrated CK Chondrite. *Meteoritics & Planetary Science* 53: 2165–80.

Dunn, T. L., Gross, J., Ivanova, M. A., Runyon, S. E., and Bruck, A. M. 2016. Magnetite in the Unequilibrated CK Chondrites: Implications for Metamorphism and New Insights into the Relationship between the CV and CK Chondrites. *Meteoritics & Planetary Science* 51: 1701–20.

Frank, D. R., Zolensky, M. E., and Le, L. 2014. Olivine in Terminal Particles of Stardust Aerogel Tracks and Analogous Grains in Chondrite Matrix. *Geochimica et Cosmochimica Acta* 142: 240–259.

Friedrich, J. M., Weisberg, M. K., Ebel, D. S., Biltz, A. E., Corbett, B. M., Iotzov, I. V., Khan, W. S., and Wolman, M. D. 2015. Chondrule Size and Related Physical Properties: A Compilation and Evaluation of Current Data across all Meteorite Groups. *Chemie der Erde* 75: 419–443.

Fukuda, K., Beard, B. L., Dunlap, D. R., Spicuzza, M. J., Fournelle, J. H., Wadhwa, M., and Kita, N. T. 2020. Magnesium Isotope Analysis of Olivine and Pyroxene by SIMS: Evaluation of Matrix Effects. *Chemical Geology* 540: 119482.

Fukuda, K., Brownlee, D. E., Joswiak, D. J., Tenner, T. J., Kimura, M., and Kita, N. T. 2021. Correlated Isotopic and Chemical Evidence for Condensation Origins of Olivine in Comet 81P/Wild 2 and in AOAs from CV and CO Chondrites. *Geochimica et Cosmochimica Acta* 293: 544–574.

Fukuda, K., Tenner, T. J., Kimura, M., Tomioka, N., Siron, G., Ushikubo, T., Chaumard, N., Hertwig, A. T., and Kita, N. T. 2022. A Temporal Shift of Chondrule Generation from the Inner to Outer Solar System Inferred from Oxygen Isotopes and Al-Mg Chronology of Chondrules from Primitive CM and CO Chondrites. *Geochimica et Cosmochimica Acta* 322: 194–226.

Geiger, T., and Bischoff, A. 1991. The CK Chondrites: Conditions of Parent Body Metamorphism (Abstract). *Meteoritics* 26: 337.

Gerber, S., Burkhardt, C., Budde, G., Metzler, K., and Kleine, T. 2017. Mixing and Transport of Dust in the Early Solar Nebula as Inferred from Titanium Isotope Variations among Chondrules. *The Astrophysical Journal* 841: L17.

Giletti, B. J., Semet, M. P., and Yund, R. A. 1978. Studies in Diffusion-III. Oxygen in Feldspars: An Ion Microprobe Determination. *Geochimica et Cosmochimica Acta* 42: 45–57.

Greenwood, R. C., Franchi, I. A., Kearsley, A. T., and Alard, O. 2010. The Relationship Between CK and CV Chondrites. *Geochimica et Cosmochimica Acta* 74: 1684–1705.

Haugbølle, T., Weber, P., Wielandt, D. P., Benítez-Llambay, P., Bizzarro, M., Gressel, O., and Pessah, M. E. 2019. Probing the Protosolar Disk Using Dust Filtering at Gaps in the Early Solar System. *The Astronomical Journal* 158: 55.

Heck, P. R., Ushikubo, T., Schmitz, B., Kita, N. T., Spicuzza, M. J., and Valley, J. W. 2010. A Single Asteroidal Source for Extraterrestrial Ordovician Chromite Grains from Sweden and China: High-Precision Oxygen Three-Isotope SIMS Analysis. *Geochimica et Cosmochimica Acta* 74: 497–509.

Hellmann, J. L., Schneider, J. M., Wölfer, E., Drążkowska, J., Jansen, C. A., Hopp, T., Burkhardt, C., and Kleine, T. 2023. Origin of Isotopic Diversity among Carbonaceous Chondrites. *The Astrophysical Journal Letters* 946: L34.

Hertwig, A. T., Defouilloy, C., and Kita, N. T. 2018. Formation of Chondrules in a Moderately High Dust Enriched Disk: Evidence from Oxygen Isotopes of Chondrules from the Kaba CV3 Chondrite. *Geochimica et Cosmochimica Acta* 224: 116–131.

Hertwig, A. T., Kimura, M., Defouilloy, C., and Kita, N. T. 2019. Oxygen Isotope Systematics of Chondrule Olivine, Pyroxene, and Plagioclase in One of the most Pristine $CV3_{Red}$ Chondrites (Northwest Africa 8613). *Meteoritics & Planetary Science* 54: 2666–85.

Hertwig, A. T., Kimura, M., Ushikubo, T., Defouilloy, C., and Kita, N. T. 2019. The ^{26}Al-^{26}Mg Systematics of FeO-Rich Chondrules from Acfer 094: Two Chondrule Generations Distinct in Age and Oxygen Isotope Ratios. *Geochimica et Cosmochimica Acta* 253: 111–126.

Hibiya, Y., Iizuka, T., Yamashita, K., Yoneda, S., and Yamakawa, A. 2019. Sequential Chemical Separation of Cr and Ti from a Single Digest for High-Precision Isotope Measurements of Planetary Materials. *Geostandards and Geoanalytical Research* 43: 133–145.

Hiyagon, H., and Hashimoto, A. 1999. ^{16}O Excesses in Olivine Inclusions in Yamato-86009 and Murchison Chondrites and their Relation to CAIs. *Science* 283: 828–831.

Ito, M., and Ganguly, J. 2006. Diffusion Kinetics of Cr in Olivine and ^{53}Mn-^{53}Cr Thermochronology of Early Solar System Objects. *Geochimica et Cosmochimica Acta* 70: 799–809.

Jabeen, I., Kusakabe, M., Nagao, K., and Ali, A. 2019. Oxygen Isotope Signatures in Bulk Chondrules: Implications for the Aqueous Alteration and Thermal Metamorphism on the Allende CV3 Parent Body. *Meteoritics & Planetary Science* 54: 431–451.

Jacquet, E. 2021. Collisions and Compositional Variability in Chondrule-Forming Events. *Geochimica et Cosmochimica Acta* 296: 18–37.

Jaoul, O., Froidevaux, C., Durham, W. B., and Michaut, M. 1980. Oxygen Self-Diffusion in Forsterite: Implications for the High-Temperature Creep Mechanism. *Earth and Planetary Science Letters* 47: 391–97.

Jollands, M. C., O'Neill, H. S. C., Van Orman, J. A., Berry, A. J., Hermann, J., Newville, M., and Lanzirotti, A. 2018. Substitution and Diffusion of Cr^{2+} and Cr^{3+} in Synthetic Forsterite and Natural Olivine at 1200–1500°C and 1 bar. *Geochimica et Cosmochimica Acta* 220: 407–428.

Jones, R. H. 1996. FeO-Rich, Porphyritic Pyroxene Chondrules in Unequilibrated Ordinary Chondrites. *Geochimica et Cosmochimica Acta* 60: 3115–17.

Joswiak, D. J., Brownlee, D. E., Nguyen, A. N., and Messenger, S. 2017. Refractory Materials in Comet Samples. *Meteoritics & Planetary Science* 52: 1612–48.

Kadlag, Y., Becker, H., and Harbott, A. 2019. Cr Isotopes in Physically Separated Components of the Allende CV3 and Murchison CM2 Chondrites: Implications for Isotopic Heterogeneity in the Solar Nebula and Parent Body Processes. *Meteoritics & Planetary Science* 54: 2116–31.

Kastelle, C. R., Helser, T. E., McKay, J. L., Johnston, C. G., Anderl, D. M., Matta, M. E., and Nichol, D. G. 2017. Age Validation of Pacific Cod (Gadus Macrocephalus) Using High-Resolution Stable Oxygen Isotope ($\delta^{18}O$) Chronologies in Otoliths. *Fisheries Research* 185: 43–53.

Kita, N. T., Nagahara, H., Tachibana, S., Tomomura, S., Spicuzza, M. J., Fournelle, J. H., and Valley, J. W. 2010. High Precision SIMS Oxygen Three Isotope Study of Chondrules in LL3 Chondrites: Role of Ambient Gas During Chondrule Formation. *Geochimica et Cosmochimica Acta* 74: 6610–35.

Kita, N. T., Nagahara, H., Togashi, S., and Morishita, Y. 2000. A Short Duration of Chondrule Formation in the Solar Nebula: Evidence from ^{26}Al in Semarkona Ferromagnesian Chondrules. *Geochimica et Cosmochimica Acta* 64: 3913–22.

Kleine, T., Budde, G., Burkhardt, C., Kruijer, T. S., Worsham, E. A., Morbidelli, A., and Nimmo, F. 2020. The Non-Carbonaceous–Carbonaceous Meteorite Dichotomy. *Space Science Reviews* 216: 55.

Kööp, L., Davis, A. M., Nakashima, D., Park, C., Krot, A. N., Nagashima, K., Tenner, T. J., Heck, P. R., and Kita, N. T. 2016. A Link Between Oxygen, Calcium and Titanium Isotopes in ^{26}Al-Poor Hibonite-Rich CAIs from Murchison and Implications for the Heterogeneity of Dust Reservoirs in the Solar Nebula. *Geochimica et Cosmochimica Acta* 189: 70–95.

Krot, A. N. 2019. Refractory Inclusions in Carbonaceous Chondrites: Records of Early Solar System Processes. *Meteoritics & Planetary Science* 54: 1647–91.

Krot, A. N., Fagan, T. J., Keil, K., McKeegan, K. D., Sahijpal, S., Hutcheon, I. D., Petaev, M. I., and Yurimoto, H. 2004. Ca,Al-Rich Inclusions, Amoeboid Olivine Aggregates, and Al-Rich Chondrules from the Unique Carbonaceous Chondrite Acfer 094: I. Mineralogy and Petrology. *Geochimica et Cosmochimica Acta* 68: 2167–84.

Krot, A. N., Hutcheon, I. D., and Keil, K. 2002. Plagioclase-Rich Chondrules in the Reduced CV Chondrites: Evidence for Complex Formation History and Genetic Links between Calcium-Aluminum-Rich Inclusions and Ferromagnesian Chondrules. *Meteoritics & Planetary Science* 37: 155–182.

Krot, A. N., and Keil, K. 2002. Anorthite Rich Chondrules in CR and CH Carbonaceous Chondrites: Genetic Link between CAIs and Ferromagnesian Chondrules. *Meteoritics & Planetary Science* 37: 91–111.

Krot, A. N., Libourel, G., and Chaussidon, M. 2006. Oxygen Isotope Compositions of Chondrules in CR Chondrites. *Geochimica et Cosmochimica Acta* 70: 767–779.

Krot, A. N., and Nagashima, K. 2016. Evidence for Oxygen-Isotope Exchange in Chondrules and Refractory Inclusions during Fluid-Rock Interaction on the CV Chondrite Parent Body In 79th Annual Meeting of the Meteoritical Society, p. 6014.

Krot, A. N., Nagashima, K., Fintor, K., and Pál-Molnár, E. 2019. Evidence for Oxygen-Isotope Exchange in Refractory Inclusions from Kaba (CV3.1) Carbonaceous Chondrite During Fluid-Rock Interaction on the CV Parent Asteroid. *Geochimica et Cosmochimica Acta* 246: 419–435.

Krot, A. N., Petaev, M. I., Scott, E. R. D., Choi, B. G., Zolensky, M. E., and Keil, K. 1998. Progressive Alteration in CV3 Chondrites: More Evidence for Asteroidal Alteration. *Meteoritics & Planetary Science* 33: 1065–85.

Krot, A. N., Scott, E. R. D., and Zolensky, M. E. 1995. Mineralogical and Chemical Modification of Components in CV3 Chondrites: Nebular or Asteroidal Processing? *Meteoritics* 30: 748–775.

Krot, A. N., and Wasson, J. T. 1995. Igneous rims on low-FeO and high-FeO chondrules in ordinary chondrites. *Geochimica et Cosmochimica Acta* 59: 4951–66.

Kruijer, T. S., Burkhardt, C., Budde, G., and Kleine, T. 2017. Age of Jupiter Inferred from the Distinct Genetics and Formation Times of Meteorites. *Proceedings of the National Academy of Sciences of the United States of America* 114: 6712–16.

Kruijer, T. S., Kleine, T., and Borg, L. E. 2020. The Great Isotopic Dichotomy of the Early Solar System. *Nature Astronomy* 4: 32–40.

Leya, I., Schönbächler, M., Krähenbühl, U., and Halliday, A. N. 2009. New Titanium Isotope Data for Allende and Efremovka CAIs. *Astrophysical Journal* 702: 1118–26.

Leya, I., Schönbächler, M., Wiechert, U., Krähenbühl, U., and Halliday, A. N. 2007. High Precision Titanium Isotope Measurements on Geological Samples by High Resolution MC-ICPMS. *International Journal of Mass Spectrometry* 262: 247–255.

Lichtenberg, T., Drążkowska, J., Schönbächler, M., Golabek, G. J., and Hands, T. O. 2021. Bifurcation of Planetary Building Blocks during Solar System Formation. *Science* 371: 365–370.

MacPherson, G. J. 2014. Calcium-Aluminum-Rich Inclusions in Chondritic Meteorites. In *Treatise on Geochemistry*, edited by H. Holland, and K. Turekian, 2nd ed., 139–179. Oxford: Elsevier.

MacPherson, G. J., and Huss, G. R. 2005. Petrogenesis of Al-Rich Chondrules: Evidence from Bulk Compositions and Phase Equilibria. *Geochimica et Cosmochimica Acta* 69: 3099–3127.

Marrocchi, Y., Euverte, R., Villeneuve, J., Batanova, V., Welsch, B., Ferrière, L., and Jacquet, E. 2019. Formation of CV Chondrules by Recycling of Amoeboid Olivine Aggregate-like Precursors. *Geochimica et Cosmochimica Acta* 247: 121–141.

Marrocchi, Y., Villeneuve, J., Batanova, V., Piani, L., and Jacquet, E. 2018. Oxygen Isotopic Diversity of Chondrule Precursors and the Nebular Origin of Chondrules. *Earth and Planetary Science Letters* 496: 132–141.

Maruyama, S., and Yurimoto, H. 2003. Relationship among O, Mg Isotopes and the Petrography of Two Spinel-Bearing Compound Chondrules. *Geochimica et Cosmochimica Acta* 67: 3943–57.

Maruyama, S., Yurimoto, H., and Sueno, S. 1999. Oxygen Isotope Evidence Regarding the Formation of Spinel-Bearing Chondrules. *Earth and Planetary Science Letters* 169: 165–171.

Miller, K. E., Lauretta, D. S., Connolly, H. C., Berger, E. L., Nagashima, K., and Domanik, K. 2017. Formation of Unequilibrated R Chondrite Chondrules and Opaque Phases. *Geochimica et Cosmochimica Acta* 209: 24–50.

Nagahara, H. 1981. Evidence for Secondary Origin of Chondrules. *Nature* 292: 135–36.

Nagashima, K., Krot, A. N., and Huss, G. R. 2015. Oxygen-Isotope Compositions of Chondrule Phenocrysts and Matrix Grains in Kakangari K-Grouplet Chondrite: Implication to a Chondrule-Matrix Genetic Relationship. *Geochimica et Cosmochimica Acta* 151: 49–67.

Nagashima, K., Krot, A. N., and Komatsu, M. 2017. ^{26}Al–^{26}Mg Systematics in Chondrules from Kaba and Yamato 980145 CV3 Carbonaceous Chondrites. *Geochimica et Cosmochimica Acta* 201: 303–319.

Nakashima, D., Ushikubo, T., Joswiak, D. J., Brownlee, D. E., Matrajt, G., Weisberg, M. K., Zolensky, M. E., and Kita, N. T. 2012. Oxygen Isotopes in Crystalline Silicates of Comet Wild 2: A Comparison of Oxygen Isotope Systematics Between Wild 2 Particles and Chondritic Materials. *Earth and Planetary Science Letters* 357–358: 355–365.

Niederer, F. R., Papanastassiou, D. A., and Wasserburg, G. J. 1981. The Isotopic Composition of Titanium in the Allende and Leoville Meteorites. *Geochimica et Cosmochimica Acta* 45: 1017–31.

Olsen, M. B., Wielandt, D., Schiller, M., Van Kooten, E. M. M. E., and Bizzarro, M. 2016. Magnesium and ^{54}Cr Isotope Compositions of Carbonaceous Chondrite Chondrules—Insights into Early Disk Processes. *Geochimica et Cosmochimica Acta* 191: 118–138.

Pape, J., Mezger, K., Bouvier, A. S., and Baumgartner, L. P. 2019. Time and Duration of Chondrule Formation: Constraints from ^{26}Al-^{26}Mg Ages of Individual Chondrules. *Geochimica et Cosmochimica Acta* 244: 416–436.

Piralla, M., Villeneuve, J., Batanova, V., Jacquet, E., and Marrocchi, Y. 2021. Conditions of Chondrule Formation in Ordinary Chondrites. *Geochimica et Cosmochimica Acta* 313: 295–312.

Piralla, M., Villeneuve, J., Schnuriger, N., Bekaert, D. V., and Marrocchi, Y. 2023. A Unified Chronology of Dust Formation in the Early Solar System. *Icarus* 394: 115427.

Rambaldi, E. R. 1981. Relict Grains in Chondrules. *Nature* 293: 558–561.

Render, J., Ebert, S., Burkhardt, C., Kleine, T., and Brennecka, G. A. 2019. Titanium Isotopic Evidence for a Shared Genetic Heritage of Refractory Inclusions from Different Carbonaceous Chondrites. *Geochimica et Cosmochimica Acta* 254: 40–53.

Righter, K., Jakubek, R. S., Fries, M. D., Schutt, J., Pando, K., and Harrington, R. 2023. Assessment of Petrologic Subtypes, Subgroups, and Pairing within CV Chondrites in the US Antarctic Meteorite Collection. *Meteoritics & Planetary Science* 58: 25–40.

Rubin, A. E. 1984. Coarse-Grained Chondrule Rims in Type 3 Chondrites. *Geochimica et Cosmochimica Acta* 48: 1779–89.

Rubin, A. E. 2010. Physical Properties of Chondrules in Different Chondrite Groups: Implications for Multiple

Melting Events in Dusty Environments. *Geochimica et Cosmochimica Acta* 74: 4807–28.

Rubin, A. E., and Wasson, J. T. 2005. Non-spherical Lobate Chondrules in CO3.0 Y-81020: General Implications for the Formation of Low-FeO Porphyritic Chondrules in CO Chondrites. *Geochimica et Cosmochimica Acta* 69: 211–220.

Rudraswami, N. G., Ushikubo, T., Nakashima, D., and Kita, N. T. 2011. Oxygen Isotope Systematics of Chondrules in the Allende CV3 Chondrite: High Precision Ion Microprobe Studies. *Geochimica et Cosmochimica Acta* 75: 7596–7611.

Russell, S. S., Zolensky, M. E., Righter, K., Folco, L., Jones, R. H., Connolly, H. C. J., Grady, M. M., and Grossman, J. N. 2005. The Meteoritical Bulletin, No. 89, 2005 September. *Meteoritics & Planetary Science* 40: A201–A263.

Ryerson, F. J., and McKeegan, K. D. 1994. Determination of Oxygen Self-Diffusion in åkermanite, Anorthite, Diopside, and Spinel: Implications for Oxygen Isotopic Anomalies and the Thermal Histories of Ca-Al-Rich Inclusions. *Geochimica et Cosmochimica Acta* 58: 3713–34.

Sanders, I. S., and Scott, E. R. D. 2012. The Origin of Chondrules and Chondrites: Debris from Low-Velocity Impacts Between Molten Planetesimals? *Meteoritics & Planetary Science* 47: 2170–92.

Sano, Y., Takada, M., Takahata, N., Fujiya, W., and Sugiura, N. 2014. Ion Microprobe Al-Mg Dating of Single Plagioclase Grains in an Efremovka Chondrule. *Geochemical Journal* 48: 133–144.

Schiller, M., Bizzarro, M., and Fernandes, V. A. 2018. Isotopic Evolution of the Protoplanetary Disk and the Building Blocks of Earth and the Moon. *Nature* 555: 507–510.

Schiller, M., Bizzarro, M., and Siebert, J. 2020. Iron Isotope Evidence for Very Rapid Accretion and Differentiation of the Proto-Earth. *Science Advances* 6: eaay7604.

Schneider, J. M., Burkhardt, C., Marrocchi, Y., Brennecka, G. A., and Kleine, T. 2020. Early Evolution of the Solar Accretion Disk Inferred from Cr-Ti-O Isotopes in Individual Chondrules. *Earth and Planetary Science Letters* 551: 116585.

Schrader, D. L., and Davidson, J. 2022. Prolonged Early Migration of Dust from the Inner Solar System to the Comet-Forming Region. *Earth and Planetary Science Letters* 589: 117552.

Schrader, D. L., Nagashima, K., Davidson, J., McCoy, T. J., Ogliore, R. C., and Fu, R. R. 2020. Outward Migration of Chondrule Fragments in the Early Solar System: O-Isotopic Evidence for Rocky Material Crossing the Jupiter Gap? *Geochimica et Cosmochimica Acta* 282: 133–155.

Sheng, Y. J., Hutcheon, I. D., and Wasserburg, G. J. 1991. Origin of Plagioclase-Olivine Inclusions in Carbonaceous Chondrites. *Geochimica et Cosmochimica Acta* 55: 581–599.

Shollenberger, Q. R., Render, J., Jordan, M. K., McCain, K. A., Ebert, S., Bischoff, A., Kleine, T., and Young, E. D. 2022. Titanium Isotope Systematics of Refractory Inclusions: Echoes of Molecular Cloud Heterogeneity. *Geochimica et Cosmochimica Acta* 324: 44–65.

Shu, F. H., Shang, H., and Lee, T. 1996. Toward an Astrophysical Theory of Chondrites. *Science* 271: 1545–52.

Simon, J. I., Jordan, M. K., Tappa, M. J., Schauble, E. A., Kohl, I. E., and Young, E. D. 2017. Calcium and Titanium Isotope Fractionation in Refractory Inclusions: Tracers of Condensation and Inheritance in the Early Solar Protoplanetary Disk. *Earth and Planetary Science Letters* 472: 277–288.

Siron, G., Fukuda, K., Kimura, M., and Kita, N. T. 2021. New Constraints from ^{26}Al–^{26}Mg Chronology of Anorthite Bearing Chondrules in Unequilibrated Ordinary Chondrites. *Geochimica et Cosmochimica Acta* 293: 103–126.

Siron, G., Fukuda, K., Kimura, M., and Kita, N. T. 2022. High Precision ^{26}Al-^{26}Mg Chronology of Chondrules in Unequilibrated Ordinary Chondrites: Evidence for Restricted Formation Ages. *Geochimica et Cosmochimica Acta* 324: 312–345.

Spandler, C., and O'Neill, H. S. C. 2009. Diffusion and Partition Coefficients of Minor and Trace Elements in San Carlos Olivine at 1,300°C with some Geochemical Implications. *Contributions to Mineralogy and Petrology* 159: 791–818.

Spitzer, F., Burkhardt, C., Budde, G., Kruijer, T. S., Morbidelli, A., and Kleine, T. 2020. Isotopic Evolution of the Inner Solar System Inferred from Molybdenum Isotopes in Meteorites. *The Astrophysical Journal Letters* 898: L2.

Spitzer, F., Burkhardt, C., Nimmo, F., and Kleine, T. 2021. Nucleosynthetic Pt Isotope Anomalies and the Hf-W Chronology of Core Formation in Inner and Outer Solar System Planetesimals. *Earth and Planetary Science Letters* 576: 117211.

Tenner, T. J., Kimura, M., and Kita, N. T. 2017. Oxygen Isotope Characteristics of Chondrules from the Yamato-82094 Ungrouped Carbonaceous Chondrite: Further Evidence for Common O-Isotope Environments Sampled among Carbonaceous Chondrites. *Meteoritics & Planetary Science* 52: 268–294.

Tenner, T. J., Ushikubo, T., Kurahashi, E., Kita, N. T., and Nagahara, H. 2013. Oxygen Isotope Systematics of Chondrule Phenocrysts from the CO3.0 Chondrite Yamato 81020: Evidence for Two Distinct Oxygen Isotope Reservoirs. *Geochimica et Cosmochimica Acta* 102: 226–245.

Torrano, Z. A., Brennecka, G. A., Mercer, C. M., Romaniello, S. J., Rai, V. K., Hines, R. R., and Wadhwa, M. 2023. Titanium and Chromium Isotopic Compositions of Calcium-Aluminum-Rich Inclusions: Implications for the Sources of Isotopic Anomalies and the Formation of Distinct Isotopic Reservoirs in the Early Solar System. *Geochimica et Cosmochimica Acta* 348: 309–322.

Trinquier, A., Birck, J., and Allegre, C. J. 2007. Widespread ^{54}Cr Heterogeneity in the Inner Solar System. *The Astrophysical Journal* 655: 1179–85.

Trinquier, A., Elliott, T., Ulfbeck, D., Coath, C., Krot, A. N., and Bizzarro, M. 2009. Origin of Nucleosynthetic Isotope Heterogeneity in the Solar Protoplanetary Disk. *Science* 324: 374–76.

Ushikubo, T., Kimura, M., Kita, N. T., and Valley, J. W. 2012. Primordial Oxygen Isotope Reservoirs of the Solar Nebula Recorded in Chondrules in Acfer 094 Carbonaceous Chondrite. *Geochimica et Cosmochimica Acta* 90: 242–264.

Ushikubo, T., Nakashima, D., Kimura, M., Tenner, T. J., and Kita, N. T. 2013. Contemporaneous formation of

chondrules in distinct oxygen isotope reservoirs. *Geochimica et Cosmochimica Acta* 109: 280–295.

Ushikubo, T., Tenner, T. J., Hiyagon, H., and Kita, N. T. 2017. A Long Duration of the ^{16}O-Rich Reservoir in the Solar Nebula, as Recorded in Fine-Grained Refractory Inclusions from the Least Metamorphosed Carbonaceous Chondrites. *Geochimica et Cosmochimica Acta* 201: 103–122.

van Kooten, E., Schiller, M., Moynier, F., Johansen, A., Haugbølle, T., and Bizzarro, M. 2021. Hybrid Accretion of Carbonaceous Chondrites by Radial Transport across the Jupiter Barrier. *The Astrophysical Journal* 910: 70.

Villeneuve, J., Chaussidon, M., and Libourel, G. 2009. Homogeneous Distribution of ^{26}Al in the Solar System from the Mg Isotopic Composition of Chondrules. *Science* 325: 985–88.

Wakaki, S., Itoh, S., Tanaka, T., and Yurimoto, H. 2013. Petrology, Trace Element Abundances and Oxygen Isotopic Compositions of a Compound CAI-Chondrule Object from Allende. *Geochimica et Cosmochimica Acta* 102: 261–279.

Warren, P. H. 2011. Stable-Isotopic Anomalies and the Accretionary Assemblage of the Earth and Mars: A Subordinate Role for Carbonaceous Chondrites. *Earth and Planetary Science Letters* 311: 93–100.

Wasson, J. T., Isa, J., and Rubin, A. E. 2013. Compositional and Petrographic Similarities of CV and CK Chondrites: A Single Group with Variations in Textures and Volatile Concentrations Attributable to Impact Heating, Crushing and Oxidation. *Geochimica et Cosmochimica Acta* 108: 45–62.

Wasson, J. T., Krot, A. N., Lee, M. S., and Rubin, A. E. 1995. Compound Chondrules. *Geochimica et Cosmochimica Acta* 59: 1847–69.

Wasson, J. T., and Rubin, A. E. 2003. Ubiquitous Low-FeO Relict Grains in Type II Chondrules and Limited Overgrowths on Phenocrysts Following the Final Melting Event. *Geochimica et Cosmochimica Acta* 67: 2239–50.

Watson, D. M., Leisenring, J. M., Furlan, E., Bohac, C. J., Sargent, B., Forrest, W. J., Calvet, N., et al. 2009. Crystalline Silicates and Dust Processing in the Protoplanetary Disks of the Taurus Young Cluster. *The Astrophysical Journal Supplement Series* 180: 84–101.

Weber, P., Benítez-Llambay, P., Gressel, O., Krapp, L., and Pessah, M. E. 2018. Characterizing the Variable Dust Permeability of Planet-Induced Gaps. *The Astrophysical Journal* 854: 153.

Weisberg, M. K., Ebel, D. S., Connolly, H. C., Kita, N. T., and Ushikubo, T. 2011. Petrology and Oxygen Isotope Compositions of Chondrules in E3 Chondrites. *Geochimica et Cosmochimica Acta* 75: 6556–69.

Weisberg, M. K., Kita, N. T., Fukuda, K., Siron, G., and Ebel, D. S. 2021. Micro-Distribution of Oxygen Isotopes in Unequilibrated Enstatite Chondrites. *Geochimica et Cosmochimica Acta* 300: 279–295.

Weisberg, M. K., McCoy, T. J., and Krot, A. N. 2006. Systematics and Evaluation of Meteorite Classification. In *Meteorites and the Early Solar System II*, edited by D. S. Lauretta, and H. Y. McSween, 19–52. Tucson: University of Arizona Press.

Whipple, F. L. 1972. On Certain Aerodynamic Processes for Asteroids and Comets. In *From Plasma to Planet, Proceedings of the Twenty-First Nobel Symposium*, edited by A. Evlius, 211–232. New York: Wiley Interscience Division.

Williams, C. D., Janney, P. E., Hines, R. R., and Wadhwa, M. 2016. Precise Titanium Isotope Compositions of Refractory Inclusions in the Allende CV3 Chondrite by LA-MC-ICPMS. *Chemical Geology* 436: 1–10.

Williams, C. D., Sanborn, M. E., Defouilloy, C., Yin, Q. Z., Kita, N. T., Ebel, D. S., Yamakawa, A., and Yamashita, K. 2020. Chondrules Reveal Large-Scale Outward Transport of Inner Solar System Materials in the Protoplanetary Disk. *Proceedings of the National Academy of Sciences of the United States of America* 117: 23426–35.

Wood, J. A. 2004. Formation of Chondritic Refractory Inclusions: The Astrophysical Setting. *Geochimica et Cosmochimica Acta* 68: 4007–21.

Yamakawa, A., Yamashita, K., Makishima, A., and Nakamura, E. 2009. Chemical Separation and Mass Spectrometry of Cr, Fe, Ni, Zn, and Cu in Terrestrial and Extraterrestrial Materials Using Thermal Ionization Mass Spectrometry. *Analytical Chemistry* 81: 9787–94.

Yin, Q. Z., and Sanborn, M. E. 2019. An Update on Disconnecting CV and CK Chondrites Parent Bodies and More. *50th Lunar and Planetary Science Conference*, abstract #3023.

Yurimoto, H., and Wasson, J. T. 2002. Extremely Rapid Cooling of a Carbonaceous-Chondrite Chondrule Containing Very ^{16}O-Rich Olivine and a ^{26}Mg-Excess. *Geochimica et Cosmochimica Acta* 66: 4355–63.

Zhang, J., Dauphas, N., Davis, A. M., and Pourmand, A. 2011. A New Method for MC-ICPMS Measurement of Titanium Isotopic Composition: Identification of Correlated Isotope Anomalies in Meteorites. *Journal of Analytical Atomic Spectrometry* 26: 2197–2205.

Zhang, M., Chaumard, N., Defouilloy, C., Nachlas, W. O., Brownlee, D. E., Joswiak, D. J., Westphal, A. J., Gainsforth, Z., Kitajima, K., and Kita, N. T. 2024. Comet 81P/Wild 2 Dust Impactors of Stardust Turnip-like Tracks Analogous to Cluster IDPs. *Geochimica et Cosmochimica Acta* 371: 214–227.

Zhang, M., Defouilloy, C., Joswiak, D. J., Brownlee, D. E., Nakashima, D., Siron, G., Kitajima, K., and Kita, N. T. 2021. Oxygen Isotope Systematics of Crystalline Silicates in a Giant Cluster IDP: A Genetic Link to Wild 2 Particles and Primitive Chondrite Chondrules. *Earth and Planetary Science Letters* 564: 116928.

Zhang, M., Fukuda, K., Spicuzza, M. J., Siron, G., Heimann, A., Hammerstrom, A. J., Kita, N. T., Ushikubo, T., and Valley, J. W. 2022. SIMS Matrix Effects in Oxygen Isotope Analysis of Olivine and Pyroxene: Application to Acfer 094 Chondrite Chondrules and Reconsideration of the Primitive Chondrule Minerals (PCM) Line. *Chemical Geology* 608: 121016.

Zhang, M., Lin, Y., Tang, G., Liu, Y., and Leya, I. 2020. Origin of Al-Rich Chondrules in CV Chondrites: Incorporation of Diverse Refractory Components into the Ferromagnesian Chondrule-Forming Region. *Geochimica et Cosmochimica Acta* 272: 198–217.

SUPPORTING INFORMATION

Additional supporting information may be found in the online version of this article.

Material S1. Description for sample preparation, oxygen isotope mixing model, and EDS data.

Figure S1. Sample preparation procedure.

Figure S2. Optical microscopic images of AL1.

Figure S3. Optical microscopic images of AL2.

Figure S4. Optical microscopic images of AL3.

Material S2. SIMS O isotope data and EDS data.

Table S1. Raw-measured O isotope data.

Table S2. O isotope data of reference materials.

Table S3. Instrumental bias.

Table S4. O isotope data of individual minerals.

Table S5. SME-EDS data.

Table S6. Compilation of chondrule size and O-Cr-Ti isotope data.

Material S3. Position of SIMS O isotope analyses.